Quaternary Research 81 (2014) 213–227

Contents lists available at ScienceDirect

Quaternary Research

journal homepage: www.elsevier.com/locate/yqres

Speleothem evidence for late Holocene climate variability and floods in Southern Greece

Martin Finné [a,b,c], Miryam Bar-Matthews [d], Karin Holmgren [a,b,c], Hanna S. Sundqvist [a,b,c], Ilias Liakopoulos [e], Qiong Zhang [a,c]

[a] Department of Physical Geography and Quaternary Geology, Stockholm University, 106 91 Stockholm, Sweden
[b] Navarino Environmental Observatory (NEO), Messinia, Greece
[c] Bolin Centre for Climate Research, Stockholm University, Sweden
[d] Geological Survey of Israel, 30 Malchei Israel Street, Jerusalem 95501, Israel
[e] Ephorate of Palaeoanthropology and Speleology of Southern Greece, Greece

ARTICLE INFO

Article history:
Received 9 September 2013
Available online 9 February 2014

Keywords:
Mediterranean
Southern Greece
late Holocene
Stalagmite
Stable isotopes
Climate variability
Flooding history
Hellenistic period

ABSTRACT

We present stable isotope data ($\delta^{18}O$, $\delta^{13}C$) from a detrital rich stalagmite from Kapsia Cave, the Peloponnese, Greece. The cave is rich in archeological remains and there are reasons to believe that flooding of the cave has directly affected humans using the cave. Using a combination of U–Th and ^{14}C dating to constrain a site-specific correction factor for ($^{232}Th/^{238}U$) detrital molar ratio, a linear age model was constructed. The age model shows that the stalagmite grew during the period from ca. 950 BC to ca. AD 830. The stable oxygen record from Kapsia indicates cyclical changes of close to 500 yr in precipitation amount, with rapid shifts towards wetter conditions followed by slowly developing aridity. Superimposed on this signal, wetter conditions are inferred around 850, 700, 500 and 400–100 BC, and around AD 160–300 and AD 770; and driest conditions are inferred to have occurred around 450 BC, AD 100–150 and AD 650. Detrital horizons in the stalagmite indicate that three major floods took place in the cave at 500 BC, 70 BC and AD 450. The stable carbon isotope record reflects changes in biological activity being a result of both climate and human activities.

Introduction

Paleoclimate data from the Peloponnese peninsula in southern Greece is scarce (Finné et al., 2011). The peninsula represents an archeologically rich and relatively well explored area that could act as an important area for investigations on the past impact of climate changes on societal development. Available paleoclimate work is mainly based on palynological studies (e.g., Kraft et al., 1980; Atherden et al., 1993; Jahns, 1993; Zangger et al., 1997; Kontopoulos and Avramidis, 2003; Urban and Fuchs, 2005; Triantaphyllou et al., 2010; Kouli, 2011). However, climate interpretation from palynological data is complex in this region due to its long history of humans altering the environment (e.g., Eastwood et al., 2007; Di Rita and Magri, 2009; Roberts et al., 2011). Limestone caves are frequently abundant and well-studied from an archeological perspective. Caves, with their well-sheltered environment, can preserve material useful, not only for archeological studies but also for paleoclimatic investigations. Provided suitable formation and preservation conditions, speleothems in caves can be precisely dated and yield high-resolution records of past variations in regional temperature, precipitation and vegetation (e.g., McDermott, 2004; Fairchild et al., 2006; Lachniet, 2009). Previous studies, incorporating paleoclimatic data from caves with archeological data, show the potential of working with this type of methods for an interdisciplinary analysis of climate–environment–society interactions (Gopher et al., 2010; Bar-Matthews and Ayalon, 2011).

We initiated a study of speleothems from Kapsia Cave in the Peloponnese, with the aim to reconstruct past climate variability and flooding history in a region that is well-studied regarding human history, and at the same site where archeological remains are abundant. Detrital horizons in the stalagmites from Kapsia Cave show signs of having been repeatedly flooded. While this may complicate the possibility of obtaining precise age information from the speleothems, improved dating techniques and the prospect of obtaining a record of past flooding events (Dorale et al., 2004), of which one might have caused the death of humans (Merdenisianos, 2005), motivated our research approach.

Here, we present U–Th and ^{14}C dating results from a detrital-rich stalagmite from the cave. Dating results are used to construct an age model that is applied to stable oxygen and carbon isotopes ($\delta^{18}O$, $\delta^{13}C$) data to yield an interpretation of climate variability during a period from ca. 950 BC to ca. AD 830. This is a period that overlaps the period when the cave is believed to have been occupied, or in use, by humans.

Setting

Kapsia Cave is situated close to the village Kapsia in Arcadia prefecture in central Peloponnese (37°37′24″N, 22°21′14″E) (Fig. 1). The

0033-5894/$ – see front matter
http://dx.doi.org/10.1016/j.yqres.2013.12.009

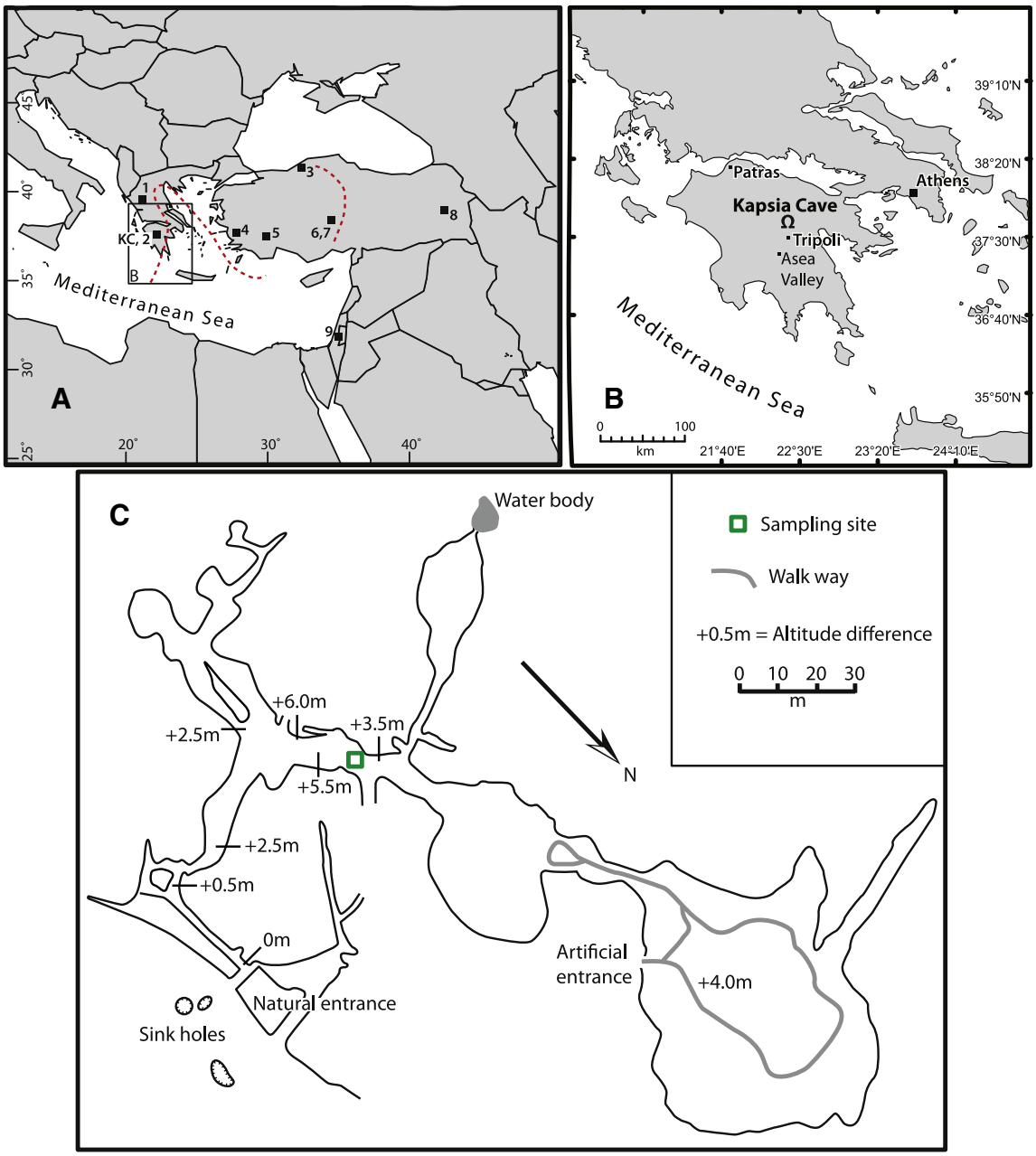

Figure 1. Map showing the location of Kapsia cave (KC) and other places mentioned in the text (A and B) and a general outline of the cave interior (C). Altitudinal differences in the cave are after map in Merdenisianos, 2005. The green square indicates the approximate sampling site of stalagmite GK-09-02. Red dashed lines in A indicate spatial differences in precipitation amounts, after Kutiel et al. (2002). Western Greece, including much of the Peloponnese, and northeastern Greece (around Thrace) and western Turkey receive more precipitation during NCPI(−) due to anomalous air flow from south to north bringing in moist air from the sea (indicated by arrows). The opposite conditions occur in, e.g., eastern Greece, Crete, eastern Turkey and the Middle East (Kutiel et al., 2002). In map A, 1: Ioannina, Frogley et al., 2001; 2: Asea Valley, Unkel et al., 2013; 3: Sofular Cave, Fleitmann et al., 2009; 4: Gölhisar, Eastwood et al., 2007; 5: Bereket basin, Kaniewski et al., 2007; 6: Eski Acigöl, Roberts et al., 2001; 7: Nar Gölu, Jones et al., 2006; 8: Soreq Cave, Bar-Matthews et al., 2003; 9: Lake Van, Wick et al., 2003.

cave entrance is located approximately 700 m asl where the Mantinea Plain meets the Pindos Mountains. The Mantinea Plain is a polje drained by 5 sinkholes (Higgins and Higgins, 1996). The cave is formed in a small limestone hill rising approximately 50 m above the plain surface. The limestones belong to the Triassic to Eocene Gavrovo–Tripolitza zone formed in shallow marine conditions (Thiébault et al., 1994; Faupl et al., 2002). Bedrock thickness above the cave is 20–30 m. The cave is beautifully decorated with numerous speleothem formations such as flow stones, curtains, stalactites, stalagmites and columns. The cave has been frequently flooded both in recent times and in the more distant past, as is clear from meter-thick clay layers on the cave floor, distinct color changes (flood marks) on speleothem surfaces (Supplemental materials, Fig. 1), and dirt horizons in sliced stalagmites (Fig. 2).

The cave environment has been monitored regularly between September 2009 and March 2013. During this time cave air temperature was stable with an average of 12.4 ± 0.5°C and the average relative humidity was around 96%. Since 2010, tourists can visit parts of the cave through an artificial entrance opened in 2004 (Fig. 1).

No excavation has been carried out in the cave with the exception of three small trial trenches (0.5 × 0.5 m) in one of the deepest chambers (Psathi, 2004). Many Neolithic (6500–3000 BC) remains from human made fires can be seen close to the natural entrance. Deeper in the cave human skulls and bones have been found, belonging to approximately 50 individuals. The human bones come from both men and women of various age, from infants to adults (Bartsiokas et al., 1981; Pitsios, 1984; Pitsios et al., 1995). Because the anthropological material

https://doi.org/10.1016/j.yqres.2013.12.009 Published online by Cambridge University Press

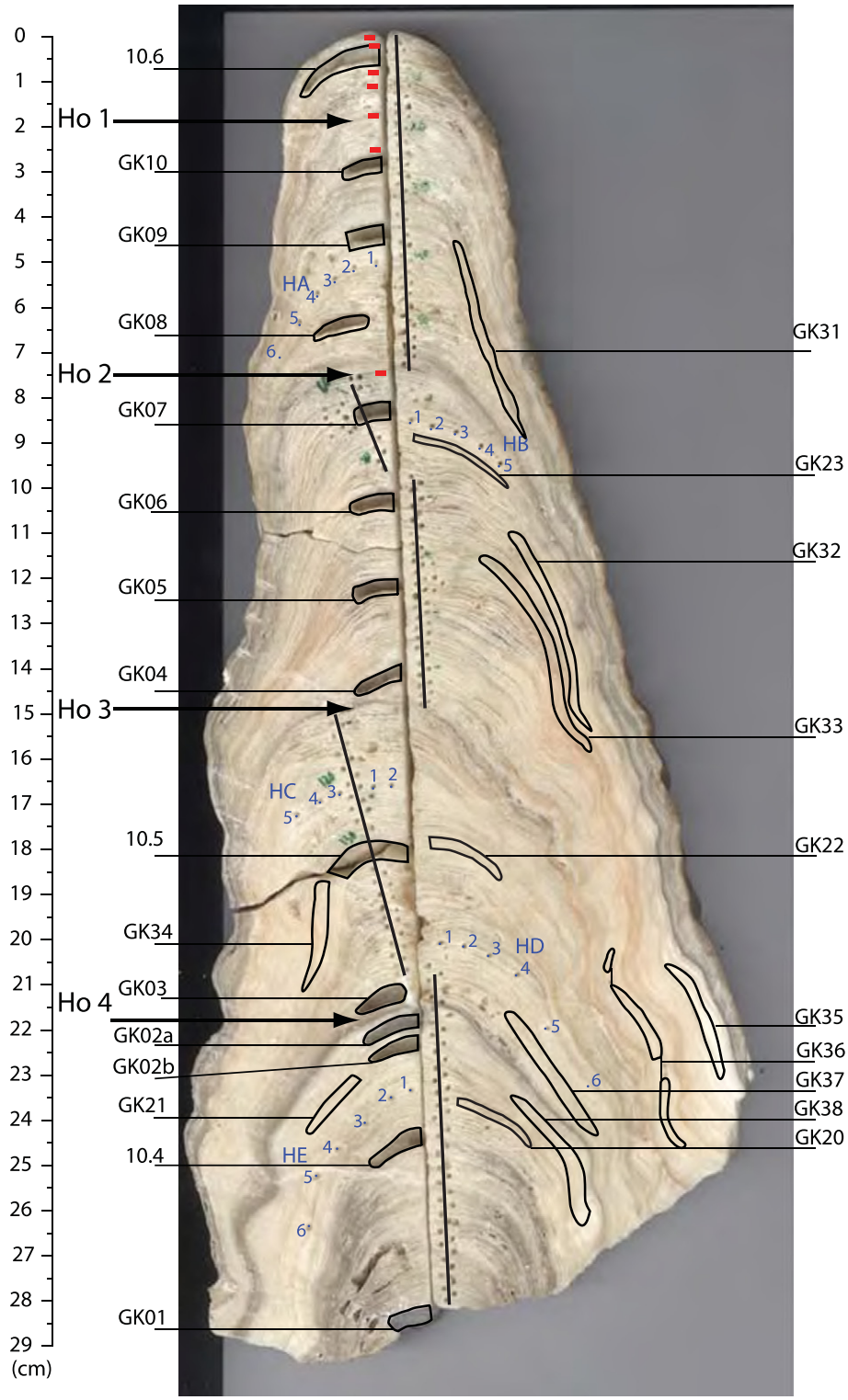

Figure 2. Sliced surface of stalagmite GK-09-02 showing sampling for U–Th dating (GK01-38 and 10.4-10.6), sampling for radiocarbon (red rectangles) sampling for stable isotopes along growth axis, sampling for Hendy tests (HA-HE) and positions of hiatuses/flood horizons (Ho 1, Ho 2, Ho 3 and Ho 4).

was not found in situ the true origin remains a conundrum. Two possible explanations have been presented by archeologists: 1) the people drowned in a flood, or starved to death when a flood sealed the natural entrance, or 2) the cave used to be a burial ground and a place of worshipping the dead and the bones found in the cave originate from already deceased persons (Merdenisianos, 2005). Deep in the cave sherds, dated to Hellenistic times (323–31 BC), have been found along with sherds and terracotta lamps dated to a period of 4th–6th century AD, and bronze coins and two bronze fibulae that are dated to the second half of the 6th century AD. It is possible that other periods of human occupation are also represented in the cave of Kapsia, since no systematic excavation has yet been carried out.

The hill above the cave is covered with vegetation dominated by oak shrubs (mainly *Quercus coccifera*) ca. 2 m high, different grass species,

https://doi.org/10.1016/j.yqres.2013.12.009 Published online by Cambridge University Press

Lamiaceae species and *Euphorbia* sp. Within the vegetation cover there are patches of bare soil and outcropping bedrock. A stand of dead tree trunks, most likely *Juniperus* sp., indicates that burning disturbs the vegetation at times and the latest major fire on the hill occurred in August 1997. The cave can be flooded at times when surface water input exceeds draining capacity of sinkholes, and the latest recorded flood was in 2001.

The regional climate is typically Mediterranean, characterized by hot dry summers and mild wet winters. Annual average air temperature for the nearest meteorological station, in Tripoli (approximately 10 km to the south, elevation 650 m), is 14.1 ± 1.4°C for the period 1951–2004. Annual average precipitation amount in Tripoli is 768 ± 393 mm for the period 1951–2008, with a great deal of year-to-year variability (Supplemental materials, Fig. 2A). Around 70–80% of the yearly precipitation falls between October and April (Dotsika et al., 2010) and snowfall occurs in higher terrain. High summer temperature and low summer precipitation lead to negative water balance for the period May to September (as indicated by the calculated water excess in Supplemental Fig. 2B). Stable isotope data in precipitation ($\delta^{18}O$ and δD) have been collected in Greece since 1960 (Argiriou and Lykoudis, 2006; Dotsika et al., 2010). The western part of the country is characterized by more precipitation and more enriched $\delta^{18}O$ values compared to the areas located in the orographic shadow to the east of the Pindos Mountains (Dotsika et al., 2010). Generally, precipitation $\delta^{18}O$ is more depleted during the winter months following surface air temperatures (Argiriou and Lykoudis, 2006). During an annual cycle a correlation between $\delta^{18}O$ depletion and rainfall amounts is evident when monthly average precipitation is below 100 mm (Argiriou and Lykoudis, 2006).

Modern climate

To provide a baseline for discussing past climate change and possible mechanism behind variability, the modern climate is briefly outlined. The North Atlantic Oscillation (NAO) influences winter precipitation and temperature of the eastern Mediterranean and Greece (Cullen and deMenocal, 2000; Türkeş and Erlat, 2003; Feidas et al., 2004). Positive (negative) NAO will create cooler and drier (warmer and wetter) conditions as less air from the North Atlantic penetrates into the region. The influence of the NAO on winter temperatures in Greece has been shown to occur mainly on a decadal scale (Feidas et al., 2004). Rainfall and temperature variability in the eastern Mediterranean depends further on the pressure difference between the North Sea and the Caspian Sea, the so called North Sea–Caspian Pattern Index (NCPI) (Kutiel and Benaroch, 2002; Kutiel et al., 2002). During a positive phase of the NCPI, NCPI(+), an anomalous circulation pattern forms in the eastern Mediterranean/Aegean Sea with a stronger component of northeasterly winds bringing cool and dry continental air into many parts of the region, including the western Peloponnese (Fig. 1). During NCPI(−) circulation tends to be stronger from the southwest favoring higher temperatures and wetter conditions (Kutiel and Benaroch, 2002; Kutiel et al., 2002). Another important control on winter temperature variability is the Mediterranean Oscillation (MO), calculated from the differences in pressure between e.g., Cairo and Algiers (Feidas et al., 2004; Harding et al., 2009). During positive MO a southward flow of cool air over Greece can be facilitated in connection to enhanced frequency and persistence of low pressures over the central Mediterranean (Feidas et al., 2004).

Materials and methods

One actively growing stalagmite, labeled GK-09-02, was collected in Kapsia Cave in September 2009. The facts that the corresponding stalactite was dripping, the stalagmite had a convex top, and modern deposition of calcite took place on equipment placed at the collection site immediately after removal of the stalagmite all strongly suggest that the stalagmite was active at the time of removal. The stalagmite was growing on an elevated plateau ca. 2 m above the cave floor. The growth location of the stalagmite is well away from both the natural and the artificial entrance in a part of the cave not accessible for tourists (Fig. 1). The height of the stalagmite is ca. 295 mm and is conically shaped (Fig. 2).

A 1-cm slab was cut parallel to the growth axis of the stalagmite using a diamond saw. The slab was then cut along the center in two equally sized parts (A and B) that were polished. Slab B was mainly devoted to sampling for stable isotopes. U–Th and radiocarbon dating samples were taken from both slabs.

The stalagmite is visibly laminated with translucent thin dark layers and thicker white deposits (Fig. 2). In areas the stalagmite is porous. Visual inspection of fabrics reveals regions with marked dark horizons at 74 mm, 149 mm, and at 214 mm (Fig. 2) from the top. Petrographic thin sections (30 μm) were produced and analyzed under Nikon Optiphot2-Pol under 25× and 100× magnification.

For radiocarbon analysis, five 2-mg samples were drilled at 3, 8, 11.5, 18 and 25 mm from the top (Fig. 2, Table 1). At 75 mm from the top, two fractions (210 mg) were analyzed: the calcite and the organic fraction. One sample (2 mg) of calcite that precipitated during the period from September 2009 to February 2010 was also analyzed to investigate if the top of the stalagmite contains an elevated ^{14}C activity that can be associated with the atomic bomb testing in the 1960s and thus provide independent evidence of recent deposition of the top of the stalagmite. Before analysis the powders were washed in de-ionized water in an ultrasonic bath. Samples were leached stepwise in 0.5 HCl to investigate possible contamination. The evolved CO_2 gas was converted into graphite using Fe-catalyst before inserted to the accelerator mass spectrometer. Radiocarbon analyses were performed at The Ångström Laboratory, Uppsala University, Sweden.

Initially 18 samples (0.5 g) were drilled for U–Th dating (Fig. 2). Based on these results a second round of 8 samples (0.3 g) was drilled closer to the sides of the stalagmite in order to avoid detrital-rich areas (Fig. 2). Additionally, the calcite, precipitated from September 2009 until February 2010 and used for ^{14}C dating, was also sampled for U–Th dating. All samples were dissolved, with a combination of 7 M HNO_3 and HF, and equilibrated with a mixed $^{229}Th/^{236}U$ spike that was calibrated with gravimetric standards (following Henderson et al., 2001). Both spiked isotopes supplied by Harwell are isotopically clean ($^{229}Th > 99.99\%$; $^{236}U = 99.97\%$). Samples were loaded onto minicolumns containing 2 ml of Bio-Rad AG 1X8 200–400 mesh resin. U was eluted by 1 M HBr and Th with 6 M HCl. U and Th solutions were evaporated to dryness and the residues dissolved in 2 ml and 5 ml of 0.1 MHNO_3, respectively.

U–Th dating was performed at the Geological Survey of Israel (GSI) using a Nu Instruments Ltd (UK) MC-ICP-MS equipped with 12 Faraday cups and 3 ion counters. Each sample was introduced to the MC-ICP-MS through an Aridus® micro-concentric desolvating nebulizer sample introducing system. The instrumental mass bias was corrected (using an exponential equation) by measuring the $^{235}U/^{238}U$ ratio and correcting with the natural $^{235}U/^{238}U$ ratio. Calibration of ion counters relative to Faraday cups was performed using several cycles of measurement with different collector configurations in each particular analysis.

Table 1
Results from radiocarbon analysis.

DFT (mm)	Sample ID	Lab. no.	a^{14}C (pMC)	^{14}C age (yr BP)
0	10	Ua-42622	101.4 ± 0.4	n.a.
3	2	Ua-41707	103.3 ± 0.4	n.a.
8	4	Ua-41761	103.7 ± 0.3	n.a.
11.5	5	Ua-42225	106.1 ± 0.4	n.a.
18	11	Ua-42623	108.9 ± 0.4	n.a.
25	6	Ua-42226	n.a.	1152 ± 30
75	12	Ua-42624	n.a.	1425 ± 30
75	$12_{organic}$	Ua-42625	n.a.	4189 ± 39

https://doi.org/10.1016/j.yqres.2013.12.009 Published online by Cambridge University Press

Isotope ratios are given as activity ratios with 2σ uncertainties (Table 2). Uncertainties are propagated from the in-run precision errors (0.4% at 2σ), weighing errors and uncertainties in spike concentrations and isotopic compositions. ^{230}Th and ^{234}U half-lives are taken from Cheng et al. (2000). Uncertainties in the half lives of the U-series isotopes are not included in the error propagation (Bar-Matthews and Ayalon, 2011; Grant et al., 2012).

For stable oxygen and carbon isotope analysis, 196 0.2-mg samples were drilled along the growth axis, using a hand-held diamond coated drill bit (Fig. 2). Additionally, 28 samples were drilled along 5 different growth laminae for testing isotopic equilibrium conditions (Hendy, 1971) (Fig. 2). Analyses were performed at the Stable Isotope Laboratory (SIL), Department of Geological Sciences, Stockholm University. The carbonate samples were flushed with argon gas in a septum-seal glass vial, and 100 μl of 99% H_3PO_4 was added to each sample for reacting to carbon dioxide. Analyses were performed using Gasbench II coupled to a Finnigan MAT 252 mass spectrometer. The reproducibility was calculated to be better than 0.15‰ for $\delta^{18}O$ and 0.07‰ for $\delta^{13}C$.

Drip water was collected from the straw stalactite directly above stalagmite GK-09-02 9 times between September 2009 and July 2012, covering all 4 seasons. Analyses were performed at SIL, Department of Geological Sciences, Stockholm University. Stable isotope analyses of hydrogen and oxygen in water were performed by a Laser Water Isotope Analyzer from Los Gatos Research; the reproducibility was calculated to be better than 0.6‰ for δD and 0.15‰ for $\delta^{18}O$. Three samples of modern calcite precipitated on equipment underneath drip site GK02 were collected in September and January 2009 and 2010, and their isotopic compositions were determined.

Results

Petrographic analysis

The stalagmite shows alternating layers of columnar calcite and open columnar calcite throughout its length (cf. Frisia and Borsato, 2010). Optical microscopy revealed a horizon marked by micrite and renucleation, with some traces of dissolution at 19 mm from the top (Horizon 1, Ho 1) (Figs. 2, 3A, B). Renucleation and incorporation of particles are visible at 149 mm (Horizon 3, Ho 3) (Figs. 3E, F) and at 214 mm (Horizon 4, Ho 4) (Figs. 3G, H). At 74 mm from the top there is a zone of ca. 3.5 mm, spanning upward, where material has been deposited in between calcite crystals but with no visible renucleation or micrite (Horizon 2, Ho 2) (Figs. 3C, D). Since the cave is prone to flooding we suggest that the horizons at 74, 149 and 214 mm from the top are the results of flooding, whereas the horizon at 19 mm may represent a period of cessation of dripping caused either by diversion of drip water or dry conditions of the aquifer.

Radiocarbon dating

Radiocarbon activity ($a^{14}C$) in the top four calcite samples (at 3, 8, 11.5 and 18 mm) show elevated values and evidence of modern carbon (Table 1) and reflect the bomb peak, demonstrating that this calcite was deposited after the year 1955 (Genty et al., 1998). The samples from 25 and 75 mm depth yielded uncalibrated ages of 1152 ± 30 and 1347 ± 30 ^{14}C yr BP, respectively. The organic residue of the sample from 75 mm gave an uncalibrated age of 4189 ± 39 ^{14}C yr BP. Two different growth periods are evident from the radiocarbon analysis, first (older) ends with the hiatus at 19 mm, and the second (younger) starts after the hiatus some time after year 1955. Since no calcite was found from the immediate pre-bomb period (i.e., 1950–1954), because of the hiatus, it was not possible to constrain the Dead Carbon Fraction (DCF) (Genty and Massault, 1997) and thus not to correct the older ^{14}C ages retrieved (Genty et al., 1999; Hodge et al., 2011). However, the ^{14}C ages from the carbonate give the oldest possible ages as a correction for DCF will yield only younger ages. The organic fraction, dated to 4189 ± 39 ^{14}C yr BP, is potentially affected by old soil organic carbon washed into the cave during a flood, explaining the offset in age between the two fractions.

Table 2
Results from U–Th dating from MC-ICP-MS analysis. Underlined samples fulfill the three criteria modified after Linge et al. (2009). Bold and underlined samples are used to discuss linear age model for stalagmite, see text for details. Corrected ages are based on a correction factor of 1.8 ± 0.25, see text for details. Errors are 2σ except corrected age error which is 2σ multiplied by a factor 3 to account for uncertainties involved in the correction. DFT is the distance from top in mm to center of milled area. All concentrations are in ppb.

Sample	DFT (mm)	^{238}U	^{238}U/^{232}Th	^{232}Th	^{230}Th/^{232}Th	^{234}U/^{232}Th	^{234}U/^{238}U	^{230}Th/^{234}U	Age (uncorrected)	Age (corrected with 1.8 ± 0.25)	BC/AD
Recent	0	313 ± 0.13	134.2	2.33 ± 0.017	9.44 ± 0.62	486.1 ± 0.73	1.01113 ± 0.0012	0.01944 ± 0.0013	2135 ± 140		
10.6	5	390 ± 0.26	73.6	5.31 ± 0.008	4.61 ± 0.07	258.5 ± 0.23	1.015077 ± 0.0008	0.01784 ± 0.0003	1957 ± 28		
GK10	30	186 ± 0.08	128.9	1.44 ± 0.003	9.96 ± 0.18	546.8 ± 1.51	1.00719 ± 0.0009	0.01821 ± 0.0003	1999 ± 40	1521 ± 168	AD 488
GK31	35	225 ± 0.17	58.1	3.87 ± 0.008	4.09 ± 0.11	238.59 ± 0.43	1.01025 ± 0.0018	0.01714 ± 0.0005	1880 ± 50		
GK09	45	206 ± 0.08	68.1	3.03 ± 0.005	7.79 ± 0.14	256.2 ± 0.22	1.02367 ± 0.0013	0.03039 ± 0.0005	3360 ± 61	2468 ± 267	459 BC
GK08	63	187 ± 0.17	26.5	7.06 ± 0.011	6.69 ± 0.05	88.5 ± 0.12	1.00252 ± 0.0019	0.07557 ± 0.0006	8556 ± 72		
GK07	82	216 ± 0.08	32.1	6.74 ± 0.012	6.81 ± 0.12	107.2 ± 0.13	1.00577 ± 0.0008	0.06348 ± 0.0011	7141 ± 129		
GK35	85	176 ± 0.11	122.2	1.44 ± 0.006	7.38 ± 0.60	503.72 ± 0.79	1.00682 ± 0.0016	0.01465 ± 0.012	1604 ± 131	1099 ± 537	AD 910
GK-23	90	217 ± 0.14	44.3	4.89 ± 0.024	9.60 ± 0.29	147.4 ± 0.25	1.00500 ± 0.0012	0.06503 ± 0.0019	7312 ± 224		
GK32	95	196 ± 0.10	54.8	3.57 ± 0.010	3.01 ± 0.12	227.45 ± 0.34	1.00453 ± 0.0015	0.01323 ± 0.0005	1448 ± 56		
GK06	102	214 ± 0.13	58.7	3.64 ± 0.009	6.39 ± 0.10	210.8 ± 0.34	1.00760 ± 0.0012	0.03034 ± 0.0005	3350 ± 52	2297 ± 213	288 BC
GK33	111	189 ± 0.18	38.3	4.93 ± 0.013	2.60 ± 0.11	147.83 ± 0.28	1.00283 ± 0.0019	0.01756 ± 0.0007	1927 ± 79		
GK05	120	217 ± 0.11	65.0	3.34 ± 0.007	5.54 ± 0.08	245.0 ± 0.39	1.01022 ± 0.0016	0.02263 ± 0.0003	2489 ± 36		
GK36	125	185 ± 0.15	170.6	1.09 ± 0.006	9.00 ± 0.51	690.74 ± 1.11	1.00116 ± 0.0016	0.01303 ± 0.0007	1426 ± 82	1063 ± 364	AD 946
GK04	140	208 ± 0.11	62.1	3.35 ± 0.010	7.16 ± 0.14	218.7 ± 0.35	1.01161 ± 0.0016	0.03272 ± 0.0007	3618 ± 73	2627 ± 315	618 BC
GK34	175	190 ± 0.13	73.8	2.58 ± 0.009	4.71 ± 0.23	288.85 ± 0.32	1.00459 ± 0.0014	0.01629 ± 0.0008	1786 ± 86		
GK-22	176	206 ± 0.18	63.2	3.27 ± 0.015	7.70 ± 0.72	220.0 ± 0.36	1.01000 ± 0.0013	0.03498 ± 0.0033	3872 ± 367	2897 ± 1638	888 BC
10.5	177	206 ± 0.12	66.1	3.12 ± 0.004	4.03 ± 0.08	264.0 ± 0.34	1.012087 ± 0.0013	0.01526 ± 0.0003	1672 ± 32		
GK03	210	197 ± 0.12	37.8	5.23 ± 0.015	5.02 ± 0.10	134.8 ± 0.14	1.00935 ± 0.0010	0.03725 ± 0.0007	4129 ± 81		
GK37	210	168 ± 0.09	99.6	1.69 ± 0.007	7.78 ± 0.25	365.54 ± 0.58	1.00832 ± 0.0009	0.02127 ± 0.0007	2339 ± 76	1720 ± 333	481 BC
GK02a	217	180 ± 0.08	14.3	12.66 ± 0.023	5.69 ± 0.07	47.1 ± 0.08	1.00547 ± 0.0012	0.12048 ± 0.0016	13,979 ± 194		
GK-21	221	199 ± 0.10	47.5	4.20 ± 0.032	9.90 ± 0.51	159.2 ± 0.15	1.01110 ± 0.0017	0.06230 ± 0.0032	6994 ± 367		
GK02b	221	199 ± 0.14	19.5	10.20 ± 0.015	7.19 ± 0.06	62.6 ± 0.08	1.00160 ± 0.0013	0.11461 ± 0.0010	13,256 ± 125		
GK38	223	169 ± 0.15	89.7	1.88 ± 0.006	7.88 ± 1.88	330.87 ± 0.52	1.00431 ± 0.0009	0.02383 ± 0.0005	2623 ± 61	1932 ± 267	AD 77
GK-20	233	188 ± 0.14	29.4	6.39 ± 0.039	8.90 ± 0.39	96.2 ± 0.22	1.00620 ± 0.0016	0.09233 ± 0.0040	10,534 ± 481		
10.4	240	184 ± 0.08	55.9	3.30 ± 0.005	8.07 ± 0.08	195.2 ± 0.14	1.014855 ± 0.0007	0.04135 ± 0.0004	4592 ± 46	3494 ± 212	1485 BC
GK01	281	182 ± 0.13	10.8	16.84 ± 0.020	4.19 ± 0.04	36.0 ± 0.09	1.00582 ± 0.0013	0.11646 ± 0.0012	13,482 ± 145		

https://doi.org/10.1016/j.yqres.2013.12.009 Published online by Cambridge University Press

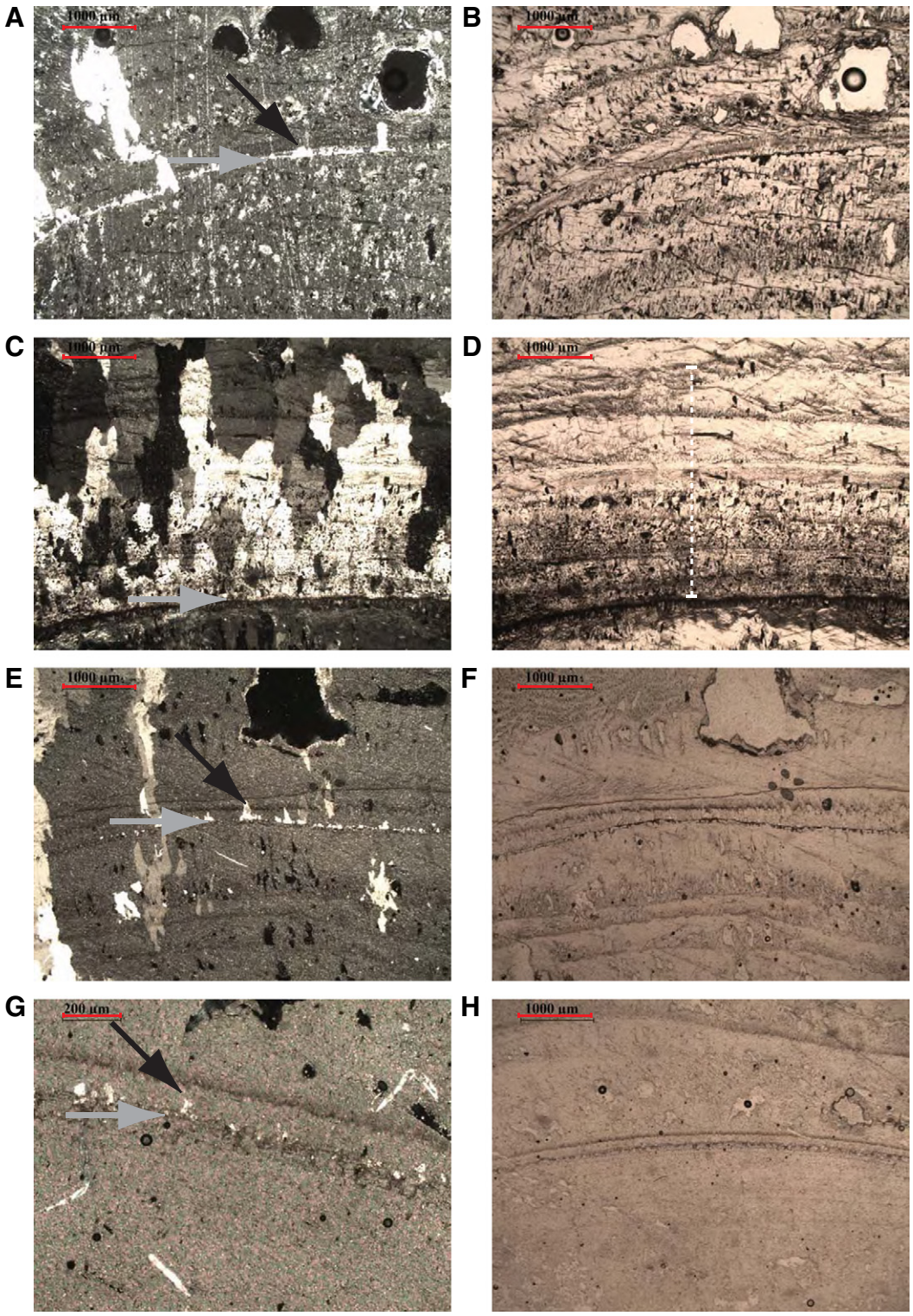

Figure 3. Plate of thin sections from stalagmite GK-09-02. Thin section has been photographed under 25x× magnification (except G, 100x), scale bars are 1000 µm (except G, 200 µm). Left side show thin sections under crossed polar and right under plane-polarized light. Black arrows show re-nucleation and gray arrows indicated the hiatus or flooded horizon. A and B show hiatus with re-nucleation at 19 mm (Ho 1). C and D show the suspected flood horizon at 74 mm (Ho 2) with a wider zone of particles incorporated into the calcite (indicated by dashed white line in D). E and F show hiatus with re-nucleation at 149 mm (Ho 3). G–H show hiatus with re-nucleation at 214 mm (Ho 4).

U–Th dating

The 26 MC-ICP-MS analyzes reveal that the stalagmite, including the recently precipitated calcite, is low in U (176–390 ppb) and high in Th, with (^{230}Th/^{232}Th) ≤9.96 (Table 2). The uncorrected age results range from 1426 ± 82 to 13,979 ± 194 yr before 2009 and do not fall in stratigraphical order. The sample of recently precipitated calcite yielded an uncorrected age of 2135 ± 140 yr before 2009. ^{232}Th is routinely monitored as an indicator of incorporation of detrital ^{230}Th into samples. The impact of initial thorium is large as indicated by the strong correlation between [^{232}Th] and uncorrected ages, $R^2 = 0.77$ (Fig. 4). A correction of all retrieved ages due to the incorporation of non-

https://doi.org/10.1016/j.yqres.2013.12.009 Published online by Cambridge University Press

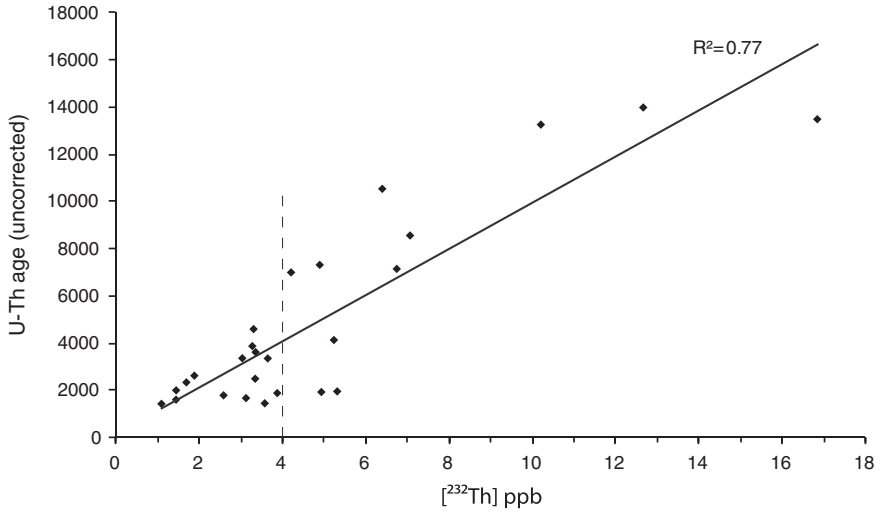

Figure 4. Correlation between [^{232}Th] and uncorrected U–Th ages showing the strong influence of a non-authigenic source of detrital thorium yielding incorrectly old ages. Dashed line delimits [^{232}Th] ≤ 4, one of the selected criteria for finding clean samples.

authigenic component of ^{230}Th is therefore required (Richards and Dorale, 2003; Hellstrom, 2006).

Stable isotopes

The Hendy tests (Hendy, 1971) show that in most cases there is no correlation between δ^{18}O and δ^{13}C along single lamina (Fig. 5A). Two tests, HA and HE, show enrichment of δ^{18}O values towards the flanks and correlation between δ^{13}C and δ^{18}O indicative of kinetic fractionation (Fig. 5A). In lamina HA there is a strong positive correlation due to a single analysis performed (HA6) along the thinnest part of the lamina. This sample is likely a mixture of several laminae. When omitting this point the correlation is weak (Fig. 5A).

The range of stable oxygen, δ^{18}O, values along the growth axis is from −4.23‰ to −6.78‰ (V-PDB) and for stable carbon, δ^{13}C, values from −6.47‰ to −10.34‰ (V-PDB). Correlation along the growth axis between δ^{13}C and δ^{18}O is low $R^2 = 0.17$ in the first growth period, between 295 mm and 19 mm, and in the second, from 19 mm to the top, $R^2 = 0.24$ (Fig. 5B).

Modern calcite precipitated underneath drip site GK02 has δ^{18}O values ranging from −4.37 to −5.12‰ (V-PDB) and δ^{13}C values from −6.94 to −8.72‰ (V-PDB) (Fig. 5C and Supplemental materials, Table 1). Drip water δ^{18}O sampled from GK02 has an average value of −6.23 ± 0.63‰ (V-SMOW) (n = 9) and is more depleted during winter compared to early summer and autumn (Supplemental materials, Table 1).

Interpretation and discussion

Age model

Incorporation of detrital thorium can change the age to a great extent in the Kapsia speleothem, as revealed by the strong correlation between [^{232}Th] and uncorrected ages (Fig. 4), and so we applied several criteria to determine which samples should be used in order to create an age model. The "best" samples were chosen in a similar empirical approach as in Linge et al. (2009) using the following criteria: [^{232}Th] ≤ 4 ppb, $(^{234}U/^{232}Th)_A \geq 100$ and [^{238}U]/[^{232}Th] ≥ 6 (underlined in Table 2). Among the 14 samples that conform to these criteria, 4 samples were omitted (GK31, GK32, GK33 and GK34 because of the very low (^{230}Th/^{232}Th) < 6), thus 10 samples remain (bold and underlined in Table 2).

Samples producing unreliable ages, i.e. GK08, GK07, GK03, GK02a, GK02b, GK20, GK21, and GK23, were all drilled adjacent to, or within, hiatus horizons. These uncorrected ages deviate from the majority of the dated samples (except GK03) and it is likely that these age determinations are affected by open system conditions caused by the hiatuses. Hence, they were discarded. Further, samples discarded are samples with low (^{230}Th/^{232}Th): 10.6, GK31, GK32, GK33, GK05, 10.5 and GK34. These are enriched in detrital component and therefore less reliable for dating. Finally sample GK01, drilled in a darker area of the stalagmite where detritus is abundant, was discarded from further analysis.

Site-specific correction factor

The need to find a site-specific correction factor for (^{232}Th/^{238}U) detrital molar ratio has been discussed by several authors (e.g., Kaufman et al., 1998; Hellstrom, 2006; Fensterer et al., 2010). Considering that samples contain high detritus and are low in uranium, the isochron method is not reliable to constrain a site-specific correction factor. In order to use isochrons to constrain a specific correction factor the detrital material needs to be homogenous, or be present in equal proportions in all samples; otherwise the isochron age determination will not be valid (Hellstrom, 2006). Using isoplot (Ludwig and Titterington, 1994) to make isochrones for coeval samples from the Kapsia stalagmite yields very large errors and also cannot be used to further constrain the corrections needed. In order to obtain the best chronology of the stalagmite from Kapsia Cave, we therefore used only the 10 "cleanest" samples and, based on their ages, discuss different possibilities to find the site-specific correction factor.

We took the following steps: First, the age of the recently precipitated calcite of 2135 ± 140 was corrected to an age close to zero by applying a high correctional factor of 0.39 (^{232}Th/^{238}U) detrital molar. By applying this correctional factor to the 10 selected samples from the stalagmite, negative values for (^{230}Th/^{234}U) are rendered in all 10 samples.

Second, we applied a correction factor of 1.8 ± 0.25 (a correction factor found for carbonate speleothems in carbonate terrain in Israel by Kaufman et al. (1998)) and this factor gave the best fit to the ^{14}C ages, with some U–Th ages being up to 400 yr older and other samples up to 400 yr younger (Fig. 6).

In summary, for building an age model, we used the 10 "cleanest" samples and corrected the age using a factor of 1.8. The 10 samples follow two different age-depth trends separated by ca. 1400 yr (Fig. 6). The younger samples are those drilled on the flanks of the stalagmite along the thinner section of the lamina and therefore represent mixture with younger laminae. The linear model is based on the average values between the two best-fit lines found for the remaining 10 samples distributed along two age-depth trends (Fig. 6). The hypothesized age

https://doi.org/10.1016/j.yqres.2013.12.009 Published online by Cambridge University Press

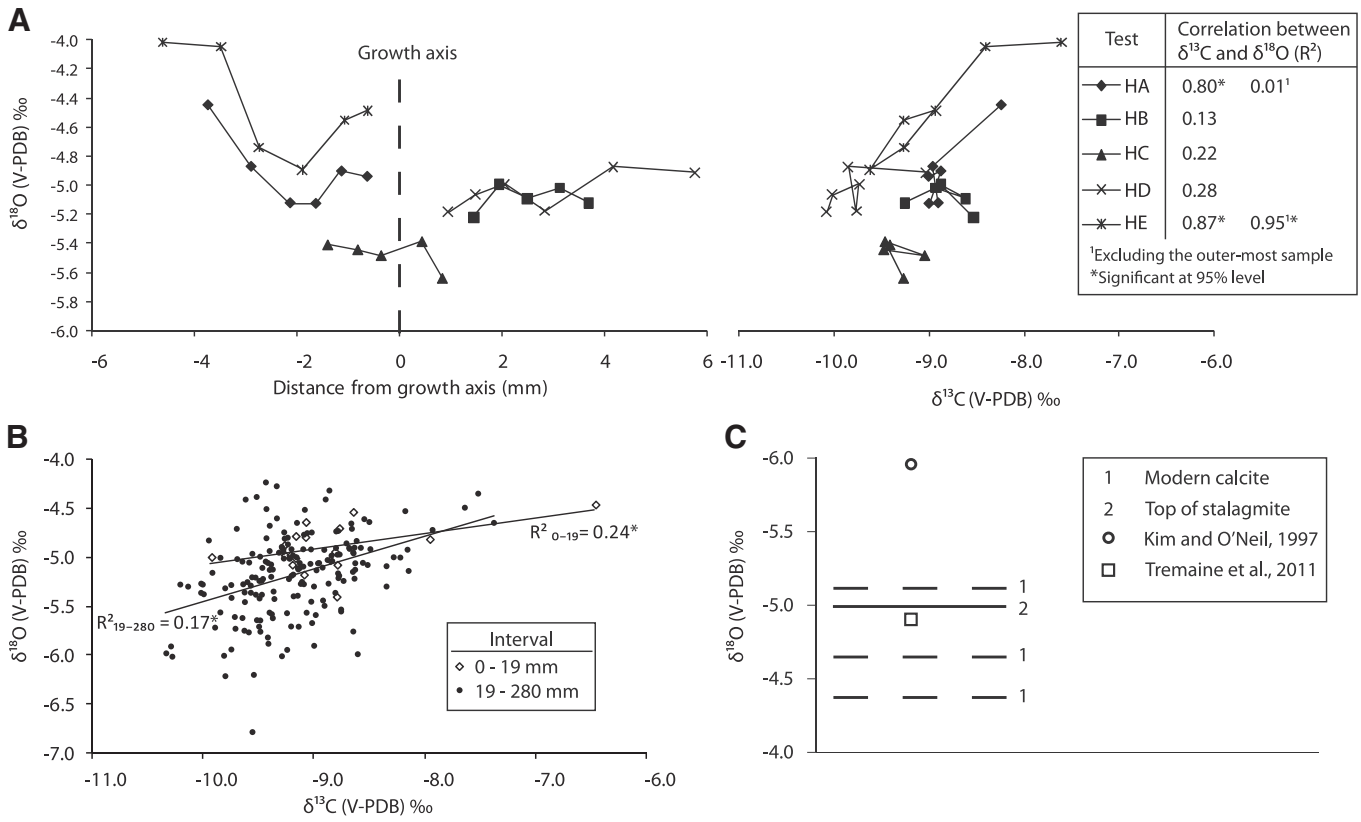

Figure 5. Evidence for equilibrium conditions. A: Hendy tests HA–HE showing little or no enrichment of $\delta^{18}O$ towards the flanks of the stalagmite (except test HE) and little or no correlation between $\delta^{13}C$ and $\delta^{18}O$ in growth lamina (except test HE). B: This test shows no correlation between $\delta^{13}C$ and $\delta^{18}O$ along the growth axis indicative of equilibrium conditions. Asterisk in A and B denote significance at 95% level. C: Comparison between measured $\delta^{18}O$ of stalagmite top and modern calcite precipitated at the collection site for GK-09-02 with calculated values for $\delta^{18}O$ in calcite precipitating under equilibrium conditions using equations suggested by Kim and O'Neil (1997) and Tremaine et al. (2011).

model suggests that the sample grew from 950 BC until AD 830, yielding a growth rate of 0.15 mm/yr and a sample resolution of the stable isotope record of approximately 10 yr.

For the second growth period covered by the top 19 mm of the stalagmite, we chose not to construct an age model, considering that we do not have any clean U–Th sample and cannot constrain the dead carbon

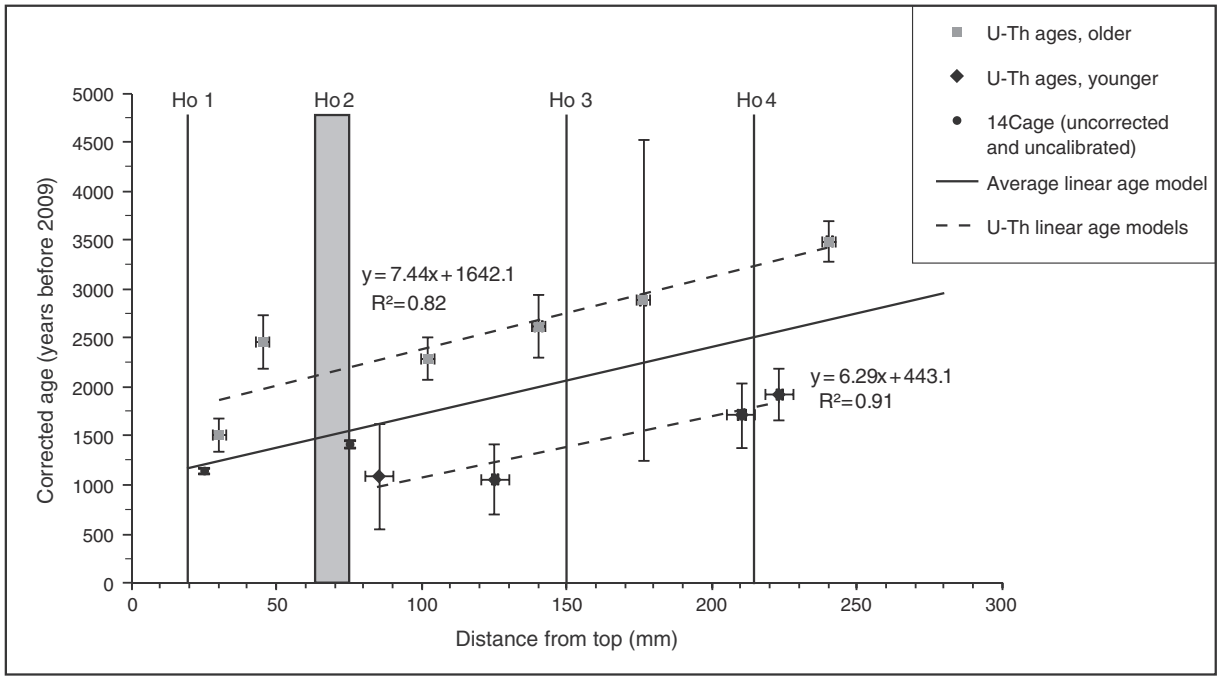

Figure 6. Linear age model using the 10 "best" U–Th ages. We use the average linear age model for discussing isotopic variability in this paper. The average linear age model is an average of values for U–Th ages, following the older best fit line and younger best fit line giving the best fit with the ^{14}C-ages.

https://doi.org/10.1016/j.yqres.2013.12.009 Published online by Cambridge University Press

fraction. We only conclude that this part of the stalagmite was deposited after AD 1955 ± 1.

Equilibrium conditions

Disequilibrium conditions can be produced by evaporation of drip water and kinetic effects including, for example, rapid degassing of CO_2 and calcite precipitation (Mickler et al., 2006). The high level of relative humidity in Kapsia cave should limit evaporation of drip water affecting $\delta^{18}O$ values, although periods of lower humidity could be more prone to evaporative fractionation effects causing high oxygen isotope values. More importantly, ventilation could lower CO_2 concentration in the cave atmosphere, which would increase CO_2 degassing from drip water resulting in enrichment of $\delta^{18}O$ (Hendy, 1971; Mickler et al., 2004; Lachniet, 2009). Slow dripping at our measure site GK02 should favor equilibrium deposition, although higher drip rates during the rainy season could lead to kinetic effects (Mickler et al., 2004).

In order to further test if calcite has been precipitated in isotopic equilibrium from the drip water, we calculated the water–calcite fractionation line by using the widely applied equations of Kim and O'Neil (1997) and Tremaine et al. (2011):

$$\text{Kim and O'Neil (1997)}: 1000\ln\alpha(\text{calcite–}H_2O) = 18.03\left(10^3\ T^{-1}\right)-32.42 \quad (1)$$

$$\text{Tremaine et al.(2011)}: 1000\ln\alpha(\text{calcite–}H_2O) = 16.1\left(10^3\ T^{-1}\right)-24.6. \quad (2)$$

By inserting the $\delta^{18}O$ values of the modern drip water that we measured in the present study into the two different equilibrium equations, we retrieve calculated average calcite $\delta^{18}O$ values of −5.96‰ (V-PDB) using Eq. (1), and a value of −4.90‰ (V-PDB) using Eq. (2) (Supplemental materials, Table 1). The theoretically retrieved value using Eq. (2) compares well with our measured values of calcite from the stalagmite top (−4.99‰ V-PDB) as well as with those of modern calcite precipitated on our equipment (−4.65, −4.37, −5.11‰ V-PDB), supporting equilibrium conditions (Fig. 5C). The relatively large deviation of 0.96‰ between our measured values and calculated values using the equation suggested by Kim and O'Neil (1997) (Fig. 5C) is in agreement with a 1.0 ± 0.5‰ offset generally found between the measured and predicted values when using this equation (McDermott et al., 2011).

The so called Hendy tests also support equilibrium conditions to a large extent, with generally poor correlation between $\delta^{18}O$ and $\delta^{13}C$ along single lamina and along the growth axis (Hendy and Wilson, 1968; Hendy, 1971). The Hendy test, HE, that does show evidence of kinetic fractionation (Fig. 5A) comes from a growth layer that is located relatively close to the flooding horizon at 214 mm and close to the dating samples that show evidence of open system conditions, suggesting that disequilibrium conditions may have affected this part of the record.

From the discussion above, we conclude that precipitation of calcite occurred under, or near, equilibrium conditions suggesting that cave air temperature and drip water isotopic composition ($\delta^{18}O$) are the main factors controlling $\delta^{18}O$ in the calcite.

Interpretation of stable isotopes $\delta^{18}O$ and $\delta^{13}C$

Drip water $\delta^{18}O$ values are controlled by $\delta^{18}O$ variations in precipitation and by processes during percolation, e.g., evaporation (e.g., Lachniet, 2009 and references therein). Potential mechanisms behind the $\delta^{18}O$ in drip water and calcite in Kapsia Cave include condensation temperature, cave air temperature, amount of precipitation, seasonality, changes in atmospheric circulation/different air masses, changes of $\delta^{18}O$ at source or change of source location.

A major shift in seasonality of precipitation, or change of precipitation source, is not likely to have occurred during the late Holocene time period covered by the analyzed stalagmite (Abrantes et al., 2012). There is little change in isotopic composition in the main precipitation sources, the Mediterranean Sea and the North Atlantic, on the time scale relevant for this study (e.g., Emeis et al., 2000; Came et al., 2007).

During the late Holocene, temperature variability in the Mediterranean region has been relatively small (e.g., Emeis et al., 2000; Emeis and Dawson, 2003; Almogi-Labin et al., 2009; Bordon et al., 2009; Finné et al., 2011). Thus the potential effect of temperature on isotope fractionation is limited. Furthermore, with increasing temperature in the atmosphere, and thus condensation temperature, precipitation $\delta^{18}O$ values will be enriched by 0.2 to 0.3‰/°C (Bard et al., 2002). This effect will, to a large extent, be counterbalanced by the fractionation changes between water and calcite causing calcite $\delta^{18}O$ to be reduced by ca. −0.24‰/°C, at low temperatures (Kim and O'Neil, 1997; Bard et al., 2002; Drysdale et al., 2005; Zanchetta et al., 2007).

Generally, depleted (enriched) $\delta^{18}O$ values in speleothems from southern Europe and the eastern Mediterranean have been interpreted in terms of increased (decreased) rainfall amounts (Bard et al., 2002;

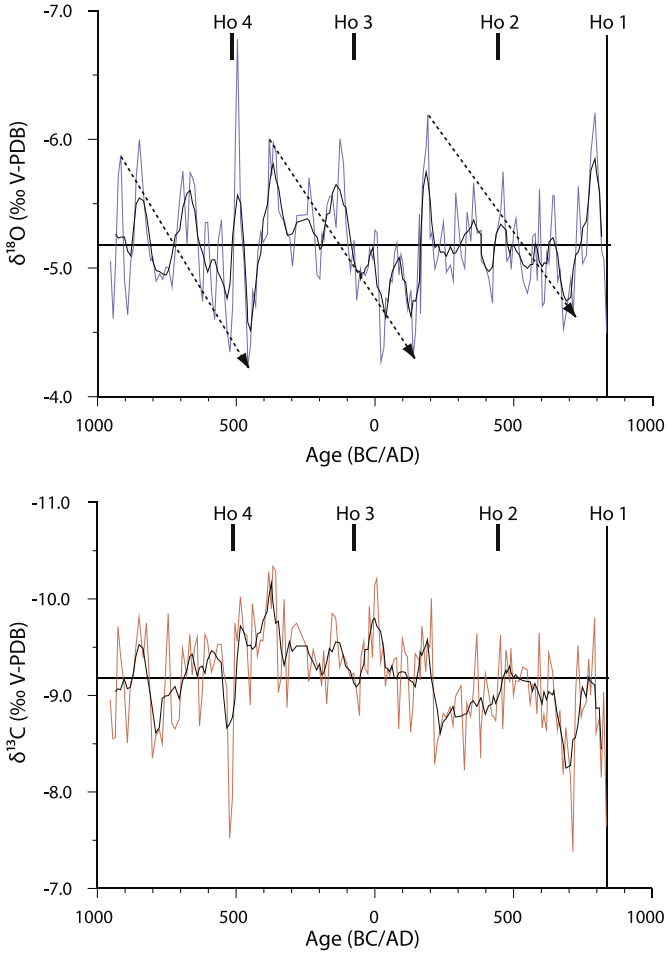

Figure 7. $\delta^{18}O$ (upper graph) and $\delta^{13}C$ (lower graph) plotted vs. age; the black line in the graphs represents the 5-point average. Note inverted y-axes. $\delta^{18}O$ is interpreted to be a proxy of rainfall amount with more depleted values representing more precipitation. $\delta^{13}C$ is interpreted to be a proxy of biological activity (more depleted values means more biological activity) as controlled, for example, by precipitation and human activities. Dashed arrows indicate periods with drying trends. Proposed flooding events are illustrated by vertical short black bars denoted Ho 4–Ho 2. The hiatus 19 mm from the top ending the record is marked by a long vertical black bar denoted Ho 1.

https://doi.org/10.1016/j.yqres.2013.12.009 Published online by Cambridge University Press

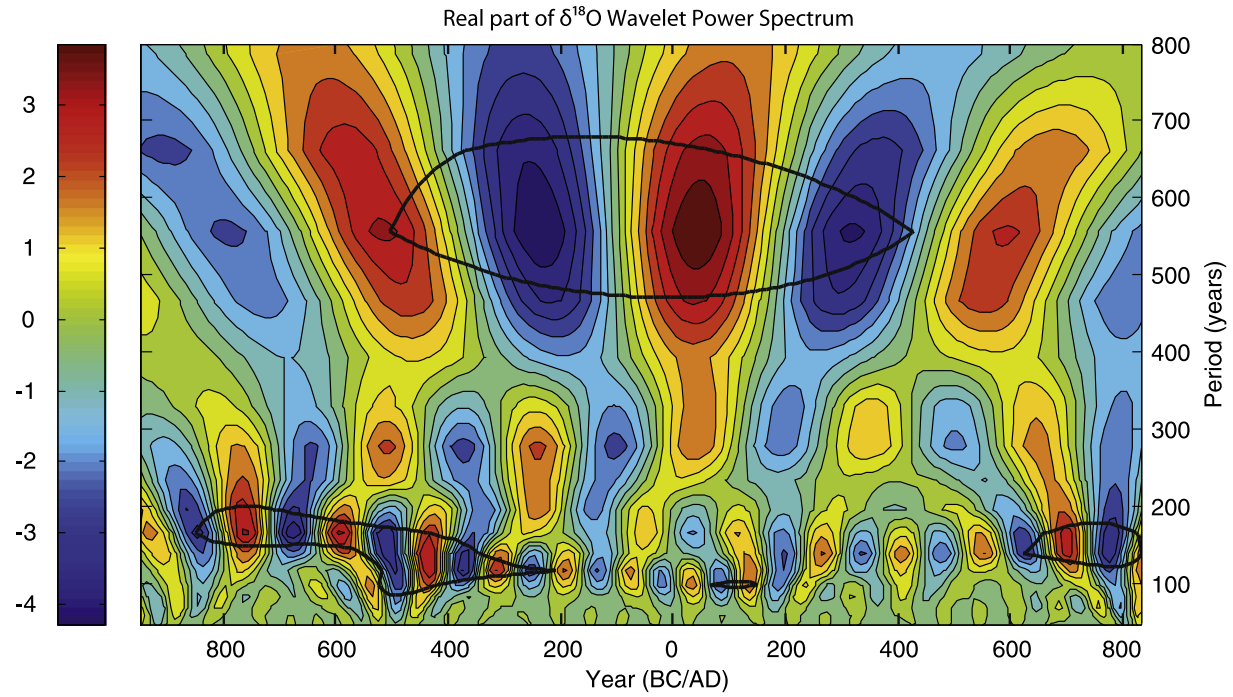

Figure 8. Wavelet analysis for the Kapsia record. The wavelet (Morlet 6) power spectrum for $\delta^{18}O$ from 954 BC to AD 834. The main oscillation periods were determined by the closed center of the real part values. The irregular time series of $\delta^{18}O$ is cubically interpolated to evenly distributed 10-year resolution to perform the wavelet power spectrum analysis. Thick black lines represent 95% significance levels, using a red noise (autoregressive lag1) background spectrum. Both low-frequency 500-year cycles and high-frequency 100- to 200-yr cycles occur throughout the record. High-frequency cycles dominate in the older and the youngest part of the Kapsia record and the low-frequency cycles in the period 500 BC to AD 450.

Bar-Matthews et al., 2003; Drysdale et al., 2005, 2006; Frisia et al., 2006; Zanchetta et al., 2007; Verheyden et al., 2008; Couchoud et al., 2009; Orland et al., 2009; Jex et al., 2010, 2011). The amount effect is a quantitatively measured control on $\delta^{18}O$ in Soreq Cave, Israel, where depletion is roughly −1‰/200–250 mm rainfall increase (Bar-Matthews et al., 2003; Orland et al., 2009). In a cave in north-western Turkey the best correlation between drip water $\delta^{18}O$ and precipitation amount was found for the period October to January (Jex et al., 2010). Frisia et al. (2006) discuss periods of enriched $\delta^{18}O$ values in terms of drier winters or more ^{18}O-enriched winter precipitation when interpreting a speleothem record from Sicily mainly based on covariation between $\delta^{18}O$ and $\delta^{13}C$ signal.

We suggest that, in common with previous findings in the Mediterranean region, the precipitation amount effect is the main control on $\delta^{18}O$ in drip water and ultimately in calcite $\delta^{18}O$ in Kapsia Cave. This means that increased (decreased) precipitation leads to more depleted (enriched) calcite $\delta^{18}O$ values. From the calculation of water excess it is evident that infiltration of water to the soil and the karst aquifer mainly occurs between October and April, assuming that runoff is negligible and that the thin soil cover cannot act as a source for seepage water when there is no rainfall (Genty and Deflandre, 1998).

Carbon isotopes in speleothems have been less utilized in climate reconstructions mainly because the carbon system presents more complexity compared to oxygen isotopes (McDermott, 2004; Cosford et al., 2009; Lambert and Aharon, 2011). In the Mediterranean region, $\delta^{13}C$ values have been interpreted as a proxy for biological activity above the cave, with increased biological activity and respiration yielding more depleted $\delta^{13}C$ values. Since the biological activity in this region is mainly controlled by amount of precipitation the $\delta^{13}C$ may in turn be used as a proxy for precipitation (Bar-Matthews et al., 2003; Frisia et al., 2006; Fleitmann et al., 2009; Göktürk et al., 2011). However, Bar-Matthews et al. (1999) have also shown that torrential downpours can lead to enriched $\delta^{13}C$ as water–soil interaction time is reduced causing very limited interaction with soil CO_2. Moreover, human actions can affect vegetation and thus constitute an important control on biological activity and ultimately $\delta^{13}C$ values. Frumkin et al. (1999) found that periods of increased deforestation caused enrichment in $\delta^{13}C$ by 2–3‰ in a speleothem from Israel. Similarly, gradual vegetation recovery has been shown to yield progressively lower $\delta^{13}C$ as input of biogenic light carbon is increased (Baldini et al., 2005). Human activity has been strong in the region of interest as shown by rich archeological records and pollen data (Fougères, 1898; Hodkinson and Hodkinson, 1981; Jahns, 1993; Parker, 2006; Triantaphyllou et al., 2010; Kouli, 2011). A strong human impact on the $\delta^{13}C$ signal could therefore be expected unless if there is co-variation between $\delta^{18}O$ and $\delta^{13}C$, as discussed by Frisia et al. (2006).

Shifts between C_3 and C_4 plant communities can also be seen in speleothems from dry areas of the eastern Mediterranean, reflected as large shifts in $\delta^{13}C$ values (e.g., Bar-Matthews et al., 1997). Speleothems deposited under C_3 dominated conditions will typically reflect more depleted $\delta^{13}C$ values, −14 to −6‰, compared to under C_4 conditions which normally range between −6 and 2‰ (McDermott, 2004).

A drier climate can also lead to reduced dripping, facilitating increased de-gassing, forcing $\delta^{13}C$ values to be enriched (Fairchild et al., 2006). Likewise, increased prior calcite precipitation in the flow path in bedrock voids may be enhanced during drier intervals causing $\delta^{13}C$ values to be more enriched. Both processes drive the $\delta^{13}C$ signal in the same directions as the biological processes outlined above.

The $\delta^{13}C$ values in the Kapsia stalagmite indicate that C_3 vegetation has constituted the dominant proportion of plant cover during deposition. This is further supported by pollen evidence from nearby Lake

Figure 9. Comparison between the record from Kapsia Cave and records from the region, arranged from west to east. For graphs, wetter conditions are up. For the bar representing Bereket basin, black color represents wetter conditions and white drier. Panel to the left shows the expected precipitation signal compared to Kapsia if NCPI is the main control on the climate (following Kutiel et al., 2002). This means that during NCPI(−) wetter conditions prevail in Kapsia as well as in those locations marked with similar, and vice versa. *In Eski Acigöl and Nar Gölu the map in Kutiel et al. (2002) is not clear about NCPI influence; however, in Jones et al. (2006) it is stated that the NCPI influence is similar.

https://doi.org/10.1016/j.yqres.2013.12.009 Published online by Cambridge University Press

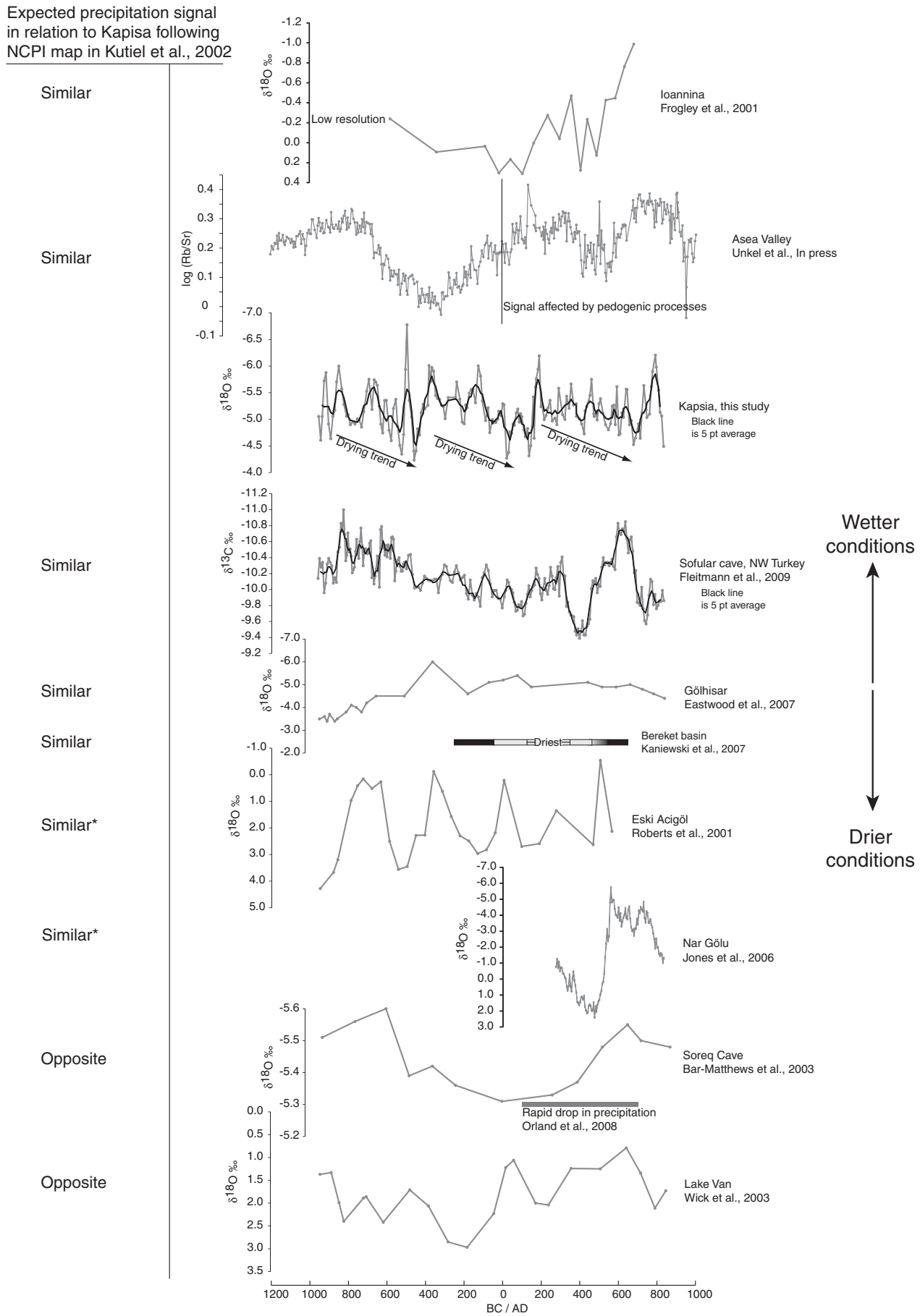

https://doi.org/10.1016/j.yqres.2013.12.009 Published online by Cambridge University Press

Lerna, and Vravron coastal marsh (Jahns, 1993; Kouli, 2011). Carbon isotopes in the Kapsia record are likely affected by biological activity, controlled by both climate and human activities, including: precipitation, temperature, deforestation, extraction of firewood and grazing. This implies that more depleted (enriched) $\delta^{13}C$ values are associated with high (low) biological activity caused by increased (reduced) precipitation or reduced (amplified) human activity. A control induced by human activities is likely stronger in the parts of the stalagmite where there is no correlation between $\delta^{18}O$ and $\delta^{13}C$.

Floods, climate and regional comparison

Using the age model established (Fig. 6), the analyzed stalagmite from Kapsia cave grew from ca. 950 BC to ca. AD 830 (or 2900 to 1120 cal yr BP). Three major floods occurred during this period, at ca. 500 BC, 70 BC and AD 450 (Ho 4 to Ho 2, Fig. 7) as indicated by petrographic analyses. There is no clear connection between floods and more depleted $\delta^{18}O$ (Fig. 7), indicating that floods are mainly controlled by the sinkholes' ability to drain water: if they are blocked during winter/spring then a flood is likely to occur. There are also ancient written records of human induced floods in Mantinea in the years 418 BC and 385 BC by blocking of sinkholes (Thucydides V 65,4; Xenophon Hellenica V 2,1–7; Diodorus XV 12,1–2, Pausanias VIII 8,7–9). However, the extent of these floods, and in particular if they reached the elevation of the stalagmite analyzed in this paper, is unclear. The flooding event at AD 450 coincides with the time when humans occupied, or used, the cave. Although it is possible that the flood caused the death of the people residing in the cave at this time, it cannot be firmly concluded from the data presented in this paper only.

A time series analysis, Morlet wavelet transform (Morlet 6) (Torrence and Compo, 1998), of the stable oxygen isotope record shows significant periodic signals (95% significance level), indicating that rainfall amount over Kapsia follows a semi-regular pattern of 500- to 600-yr cycles and of 100- to 200-yr cycles (Fig. 8). A similar pattern of close to 500-yr cycle was found in a drift-ice record from the North Atlantic associated with solar activity (Bond et al., 2001). In the eastern Mediterranean context late Holocene cycles of 500–800 yr in length have been shown to relate to surface water productivity increases connected to elevated nutrient input from the Nile (Schilman et al., 2001, 2003). The quasi-500-yr cycles evident in the Kapsia record display a pattern of more rapid shifts to wetter conditions (i.e., isotopic depletion) followed by slower changes towards drier conditions (i.e., isotopic enrichment at ca. 950–400 BC, 400 BC–AD 150 and ca. AD 150–650 (Fig. 7). Superimposed on this 500- to 600-yr cycle, a centennial variability signal (100–200 yr) occurs with wetter conditions centered around 850, 700, 500 and 400–100 BC, and around AD 160–300 and AD 770. Drier conditions are centered around 800, 550 and 450 BC, at 100 BC–AD 150, and at AD 650 (Fig. 7). Our data suggest a shift in the dominance of the frequency of the signal. During the period from ca. 950 BC to AD 300 the low-frequency signal at 500–600 yr dominates, while from AD 300 to the end of the record the 100–200 yr signal becomes dominant (Fig. 8).

The $\delta^{13}C$ signal from Kapsia generally indicates that biological activity slowly increased in the period from around 900 to around 400 BC (Fig. 7). This was then followed by a generally high biological activity with a slow decline until around AD 160 when a rapid setback is recorded by a strong enrichment in $\delta^{13}C$. After the rapid decline the biological activity remains low with a small regeneration just before AD 500 followed by very low activity around AD 700.

The $\delta^{13}C$ signal from Kapsia does not closely follow the $\delta^{18}O$, indicating that other agents than the climate are important for the biological activity above the cave. Especially, in the period from 50 BC to AD 450 correlation between oxygen and carbon isotopes is very weak. A possible explanation is that drier conditions in the interval 100 BC–AD 150 could have led to reduced human activities in the area providing a possibility for the vegetation to recover. The wetter conditions that then followed from AD 160 created an opportunity for people to increase their impact in the landscape possibly leading to the low biological activity following the rapid setback.

Pollen from Vravron marsh (ca. 150 km to the east) indicates a decline in human activities and an expansion of pine forests in the period 900 to 300 BC, which is closely matched by the $\delta^{13}C$ signal indicating increasing biological activity in the period 900–400 BC. This period is then followed by an expansion of deciduous forest from 300 BC to AD 200 but with stronger imprints of human activities in Vravron, which is also nicely matched by the record from Kapsia where biological activity is high between 450 BC and AD 160. This period of higher biological activity closely matches a period of warmer conditions often referred to as the Roman warm period, lasting between 450 BC and AD 150 (Frisia et al., 2006; Finné et al., 2011). Warmer conditions, especially during winter, could possibly create more favorable conditions for vegetation growth. From the Kapsia $\delta^{13}C$ signal it seems as if the vegetation is not recovering to previous conditions after the rapid setback at AD 160. This is most likely an indicator of sustained human activities suppressing vegetation recovery or that the drying trend from AD 150–650 evident from gradual enrichment in $\delta^{18}O$ is hampering regeneration.

Other paleoclimatic records from nearby regions, covering the same period of time, come from marine and terrestrial proxy archives (e.g., Greece, Israel, Syria and Turkey; Fig. 9). The comparison reveals a large intra-regional variability, as has been previously pointed out by Finné et al. (2011), making comparisons between records difficult. Both similarities and differences between the record from Kapsia and nearby records can be seen. The initial drying trend found in Kapsia from 950 to 450 BC is supported by a sediment record from the nearby Asea Valley (ca. 30 km), where wetter conditions lasting until 750 BC transitioned into a period of dry conditions that reached their apex around 350 BC (Unkel et al., 2013). Similarly, isotope data from Soreq Cave, Israel, suggest increasing aridity in the interval 650–450 BC followed by increased rainfall (Bar-Matthews et al., 2003; Bar-Matthews and Ayalon, 2004). In Turkey, wetter conditions are evident from around 150 to 50 BC (Roberts et al., 2001, 2008; Wick et al., 2003; Lamy et al., 2006; Kaniewski et al., 2007), which only partly matches the wet interval at Kapsia 400–100 BC. The dry interval recorded in Kapsia at around 100 BC–AD 150 followed by the wet spell at AD 150–300 has counterparts at Ioannina, NW Greece, where dry conditions are noted at 50 BC–AD 150 and wetter conditions between AD 150 and 350 (Frogley et al., 2001; Roberts et al., 2008). There is also evidence from Sofular Cave in NW Turkey (Fleitmann et al., 2009) for drier conditions followed by wetter, roughly coinciding with Kapsia. Fewer similarities are observed with Soreq Cave, Israel, where drier conditions are inferred first after 50 BC, with a rapid drop in precipitation at AD 100–700 (Orland et al., 2009). In line with Soreq cave, drier conditions are observed at Bereket Basin in western Turkey from around 40 BC with increasing aridity until AD 550 (Kaniewski et al., 2007). Dry conditions in central Turkey are further evident at AD 280 to 530 from an isotope record from Nar Gölü (lake) (Jones et al., 2006). Wetter conditions observed towards the end of the Kapsia record, starting at around AD 700, are preceded by wetter conditions starting somewhat earlier at Ioannina (Frogley et al., 2001; Roberts et al., 2008), Bereket Basin and Nar Gölü from AD 530.

These sometimes opposing, sometimes synchronous signals from the Middle East and Turkey, in comparison to records from Greece, might be explained by the relative dominance between NAO and NCPI. If NAO is the dominating control on the climate with a NAO(+) situation creating conditions of reduced anti-cyclonal activity reducing moisture in the eastern Mediterranean, a similar signal in the large scale basin would be expected. However, if NCPI is the main control, opposed moisture conditions would be expected between the central Peloponnese and western/central Turkey and the Middle East (Kutiel et al., 2002). Jones et al. (2006) hypothesize that the period from AD 530 to 1400 was dominated by negative NCPI, with wetter conditions prevailing in western Turkey and western and central Peloponnese.

https://doi.org/10.1016/j.yqres.2013.12.009 Published online by Cambridge University Press

Conclusions

We have provided the first stalagmite-based paleoclimate record for southern Greece. The record covers a near 1800-yr-long period from 950 BC to AD 830. The stable oxygen isotope signal in the stalagmite shows that the regional hydroclimate followed a semi-regular pattern of 500- to 600-yr cycles, similar to cycles found in the North Atlantic, which might be related to solar activity cycles. The cycles evident in our record include rapid shifts towards wetter conditions followed by slowly developing aridity. Centennial-scale variability in hydroclimatic conditions is superimposed on the low-frequency cycles. Wetter conditions are inferred around 850, 700, 500 and 400–100 BC, and around AD 160–300 and AD 770. Driest conditions are inferred to have occurred around 450 BC, AD 100–150 and AD 650.

Our record shows sometimes an opposing and sometimes a synchronous signal with records from the Middle East and Turkey, indicating shifts in the relative dominance between North Atlantic Oscillation and the North Sea–Caspian Pattern Index as regional climate controlling atmospheric processes.

Detrital hiatuses in the stalagmite show that floods occurred in the cave in 500 BC, 70 BC and AD 450. The latest flood may have influenced the presence of human activity in the cave, as is observed from archeological evidence from the 4th and 5th centuries AD.

Our record provides new knowledge, both about climate variability from the Peloponnese, a region where this type of data is scarce, and about local environmental conditions that might have impacted on past human activities. By adding this piece of information a better understanding of the regional climate is achieved and attempts to understand climate variability in the region does not solely have to rely on more distant paleoclimate records. This type of data further enhances the possibilities for improved analysis of the climate–society interactions over time in this archeologically rich region.

Supplementary data to this article can be found online at http://dx.doi.org/10.1016/j.yqres.2013.12.009.

Acknowledgment

This research has been carried out within the framework of the Navarino Environmental Observatory (NEO), Messinia, Greece, a cooperation between Stockholm University, the Academy of Athens and TEMES S.A. NEO is dedicated to research and education on the climate and environment of the Mediterranean region. We thank the Ephorate of Palaeoanthropology and Speleology of Southern Greece for permitting visits to and sampling in Kapsia Cave and Yannis Bassiakos for introducing us to the cave. Grigoris Rousiotis provided valuable information about the cave and the surroundings including recent floods and fires. Joylon Desmarchelier, Nikos Kalivitis, Giorgos Maneas, Meighan Boyd and Kristina Westermark assisted during field work. Heike Sigmund, Stable Isotope Laboratory (SIL), Department of Geological Sciences, Stockholm University, provided help and comments on stable isotope analyses. Silvia Frisia gave invaluable input on the petrographic analyzes. Discussions with and help from Göran Possnert, Ångströmlaboratoriet, Uppsala University, has been crucial for ^{14}C-dating and interpretations of the results. Marika Wennbom assisted with maps. Comments from Senior Editor Derek Booth and two anonymous reviewers improved the quality of the manuscript. Field work was financed by The Swedish Society for Anthropology and Geography and Albert och Maria Bergström stiftelse. Analytical work was financed by M Althins Foundation, Carl Mannerfelts Fond and Lagrelius Fond.

References

Abrantes, F., Voelker, A.H.L., Sierro, F.J., Naughton, F., Rodrigues, T., Cacho, I., Ariztegui, D., Brayshaw, D., Sicre, M.-A., Batista, L., 2012. Paleoclimate variability in the Mediterranean Region. In: Lionello, P. (Ed.), Climate of the Mediterranean Region: From the Past to the Future. Elsevier, London, pp. 1–86.

Almogi-Labin, A., Bar-Matthews, M., Shriki, D., Kolosovsky, E., Paterne, M., Schilman, B., Ayalon, A., Aizenshtat, Z., Matthews, A., 2009. Climatic variability during the last 90 ka of the southern and northern Levantine Basin as evident from marine records and speleothems. Quaternary Science Reviews 28, 2882–2896.

Argiriou, A.A., Lykoudis, S., 2006. Isotopic composition of precipitation in Greece. Journal of Hydrology 327, 486–495.

Atherden, M., Hall, J., Wright, J.C., 1993. A pollen diagram from the northeast Peloponnese, Greece: implications for vegetation history and archaeology. The Holocene 4, 351–356.

Baldini, J.U.L., McDermott, F., Baker, A., Baldini, L.M., Mattey, D.P., Railsback, L.B., 2005. Biomass effects on stalagmite growth and isotope ratios: a 20th century analogue from Wiltshire, England. Earth and Planetary Science Letters 240, 486–494.

Bard, E., Antonioli, F., Silenzi, S., 2002. Sea-level during the penultimate interglacial period based on a submerged stalagmite from Argentarola Cave (Italy). Earth and Planetary Science Letters 196, 135–146.

Bar-Matthews, M., Ayalon, A., 2004. Speleothems as palaeoclimate indicators, a case study from Soreq Cave located in the eastern Mediterranean region, Israel. In: Battarbee, R.W., Gasse, F., Stickley, C.E. (Eds.), Past Climate Variability Through Europe and Africa. Springer, Dordrecht, pp. 363–391.

Bar-Matthews, M., Ayalon, A., 2011. Mid-Holocene climate variations revealed by high-resolution speleothem records from Soreq Cave, Israel and their correlation with cultural changes. The Holocene 21, 163–171.

Bar-Matthews, M., Ayalon, A., Kaufman, A., 1997. Late Quaternary Paleoclimate in the Eastern Mediterranean Region from stable isotope analysis of speleothems at Soreq Cave, Israel. Quaternary Research 47, 155–168.

Bar-Matthews, M., Ayalon, A., Kaufman, A., Wasserburg, G.J., 1999. The eastern Mediterranean paleoclimate as a reflection of regional events: Soreq cave, Israel. Earth and Planetary Science Letters 166, 85–95.

Bar-Matthews, M., Ayalon, A., Gilmour, M., Matthews, A., Hawkesworth, C.J., 2003. Sea–land oxygen isotopic relationships from planktonic foraminifera and speleothems in the Eastern Mediterranean region and their implication for paleorainfall during interglacial intervals. Geochimica et Cosmochimica Acta 67, 3181–3199.

Bartsiokas A., Merdenisianos K., Zafeiratos K., 1981. Τα ανθρωπολογικά ευρήματα του σπηλαίου Κάψια Τριπόλεως και η ιστορία τους. (1ο Πανελλήνιο Σπηλαιολογικό Συμπόσιο. Αθήνα 1981. Δελτίο Ελληνικής Σπηλαιολογικής Εταιρείας (Ε.Σ.Ε.) XVIII 1–2, 1981–82).

Bond, G., Kromer, B., Beer, J., Muscheler, R., Evans, M.N., Showers, W., Hoffmann, S., Lotti-Bond, R., Hajdas, I., Bonani, G., 2001. Persistent solar influence on north Atlantic climate during the Holocene. Science 294, 2130–2136.

Bordon, A., Peyron, O., Lézine, A.-M., Brewer, S., Fouache, E., 2009. Pollen-inferred Late-Glacial and Holocene climate in southern Balkans (Lake Maliq). Quaternary International 200, 19–30.

Came, R.E., Oppo, D.W., McManus, J.F., 2007. Amplitude and timing of temperature and salinity variability in the subpolar North Atlantic over the past 10 k.y. Geology 35, 315–318.

Cheng, H., Edwards, R.L., Hoff, J., Gallup, C.D., Richards, D.A., Asmerom, Y., 2000. The half-lives of uranium-234 and thorium-230. Chemical Geology 169, 17–33.

Cosford, J., Qing, H., Mattey, D., Eglington, B., Zhang, M., 2009. Climatic and local effects on stalagmite δ^{13}C values at Lianhua Cave, China. Palaeogeography, Palaeoclimatology, Palaeoecology 280, 235–244.

Couchoud, I., Genty, D., Hoffmann, D., Drysdale, R., Blamart, D., 2009. Millennial-scale climate variability during the Last Interglacial recorded in a speleothem from south-western France. Quaternary Science Reviews 28, 3263–3274.

Cullen, H.M., DeMenocal, P.B., 2000. North Atlantic influence on Tigris–Euphrates streamflow. International Journal of Climatology 20, 853–863.

Di Rita, F., Magri, D., 2009. Holocene drought, deforestation and evergreen vegetation development in the central Mediterranean: a 5500 year record from Lago Alimini Piccolo, Apulia, southeast Italy. The Holocene 19, 295–306.

Dorale, J.A., Edwards, R.L., Alexander, E.C., Shen, C.-C., Richards, D.A., Cheng, H., 2004. Uranium-series dating of speleothems: current techniques, limits and applications. In: Sasowsky, I.D., Mylroie, J. (Eds.), Studies of Cave Sediments. Physical and Chemical Records of Palaeoclimate. Kluwer Academic, New York, pp. 177–197.

Dotsika, E., Lykoudis, S., Poutoukis, D., 2010. Spatial distribution of the isotopic composition of precipitation and spring water in Greece. Global and Planetary Change 71, 141–149.

Drysdale, R.N., Zanchetta, G., Hellstrom, J.C., Fallick, A.E., Zhao, J.-X., 2005. Stalagmite evidence for the onset of the Last Interglacial in southern Europe at 129 ± 1 ka. Geophysical Research Letters 32, 1–4.

Drysdale, R., Zanchetta, G., Hellstrom, J., Maas, R., Fallick, A., Pickett, M., Cartwright, I., Piccini, L., 2006. Late Holocene drought responsible for the collapse of Old World civilizations is recorded in an Italian flowstone. Geology 34, 101–104.

Eastwood, W.J., Leng, M.J., Roberts, N., Davis, B., 2007. Holocene climate change in the eastern Mediterranean region: a comparison of stable isotope and pollen data from Lake Gölhisar, southwest Turkey. Journal of Quaternary Science 22, 327–341.

Emeis, K.-C., Dawson, A.G., 2003. Holocene palaeoclimate records over Europe and the North Atlantic. The Holocene 13, 305–309.

Emeis, K.C., Struck, U., Schulz, H.M., Rosenberg, R., Bernasconi, S., Erlenkeuser, H., Sakamoto, T., Martinez-Ruiz, F., 2000. Temperature and salinity variations of Mediterranean Sea surface waters over the last 16,000 years from records of planktonic stable oxygen isotopes and alkenone unsaturation ratios. Palaeogeography, Palaeoclimatology, Palaeoecology 158, 259–280.

Fairchild, I.J., Smith, C.L., Baker, A., Fuller, L., Spötl, C., Mattey, D., McDermott, F., 2006. Modification and preservation of environmental signals in speleothems. Earth-Science Reviews 75, 105–153.

Faupl, P., Pavlopoulos, A., Migiros, G., 2002. Provenance of the Peloponnese (Greece) flysch based on heavy minerals. Geological Magazine 139, 513–524.

Feidas, H., Makrogiannis, T., Bora-Senta, E., 2004. Trend analysis of air temperature time series in Greece and their relationship with circulation using surface and satellite data: 1955–2001. Theoretical and Applied Climatology 79, 185–208.
Fensterer, C., Scholz, D., Hoffmann, D., Mangini, A., Pajón, J.M., 2010. ^{230}Th/U-dating of a late Holocene low uranium speleothem from Cuba. IOP Conf. Ser.: Earth and Environmental Science, 9 012015.
Finné, M., Holmgren, K., Sundqvist, H.S., Weiberg, E., Lindblom, M., 2011. Climate in the eastern Mediterranean, and adjacent regions, during the past 6 000 years — a review. Journal of Archaeological Science 38, 3153–3173.
Fleitmann, D., Cheng, H., Badertscher, S., Edwards, R.L., Mudelsee, M., Göktürk, O.M., Fankhauser, A., Pickering, R., Raible, C.C., Matter, A., Kramers, J., Tüysüz, O., 2009. Timing and climatic impact of Greenland interstadials recorded in stalagmites from northern Turkey. Geophysical Research Letters 36 (art. no. L19707).
Fougères, G., 1898. Mantinée et l' Arcadie orientale (Paris 1898).
Frisia, S., Borsato, A., 2010. Karst (chapter 6). Developments in Sedimentology 61 (C), 269–318.
Frisia, S., Borsato, A., Mangini, A., Spötl, C., Madonia, G., Sauro, U., 2006. Holocene climate variability in Sicily from a discontinuous stalagmite record and the Mesolithic to Neolithic transition. Quaternary Research 66, 388–400.
Frogley, M.R., Griffiths, H.I., Heaton, T.H.E., 2001. Historical biogeography and late Quaternary environmental change of Lake Pamvotis, Ioannina (north-western Greece): evidence from ostracods. Journal of Biogeography 28, 745–756.
Frumkin, A., Carmi, I., Gopher, A., Ford, D.C., Schwarcz, H.P., Tsuk, T., 1999. A Holocene millennial-scale climatic cycle from a speleothem in Nahal Qanah Cave, Israel. The Holocene 9, 677–682.
Genty, D., Deflandre, G., 1998. Drip flow variations under a stalactite of the Pere Noel cave (Belgium). Evidence of seasonal variations and air pressure constraints. Journal of Hydrology 211, 208–232.
Genty, D., Massault, M., 1997. Bomb ^{14}C recorded in laminated speleothems: calculation of dead carbon proportion. Radiocarbon 39, 33–48.
Genty, D., Vokal, B., Obelic, B., Massault, M., 1998. Bomb ^{14}C time history recorded in two modern stalagmites — importance for soil organic matter dynamics and bomb ^{14}C distribution over continents. Earth and Planetary Science Letters 160, 795–809.
Genty, D., Massault, M., Gilmour, M., Baker, A., Verheyden, S., Kepens, E., 1999. Calculation of past dead carbon proportion and variability by the comparison of AMS ^{14}C and TIMS U/Th ages on two Holocene stalagmites. Radiocarbon 41, 251–270.
Göktürk, O.M., Fleitmann, D., Badertscher, S., Cheng, H., Edwards, R.L., Leuenberger, M., Fankhauser, A., Tüysüz, O., Kramers, J., 2011. Climate on the southern Black Sea coast during the Holocene: implications from the Sofular Cave record. Quaternary Science Reviews 30, 2433–2445.
Gopher, A., Ayalon, A., Bar-Matthews, M., Barkai, R., Frumkin, A., Karkanas, P., Shahack-Gross, R., 2010. The chronology of the late Lower Paleolithic in the Levant based on U–Th ages of speleothems from Qesem Cave, Israel. Quaternary Geochronology 5, 644–656.
Grant, K.M., Rohling, E.J., Bar-Matthews, M., Ayalon, A., Medina-Elizalde, M., Bronk Ramsey, C., Satow, C., Roberts, A.P., 2012. Rapid coupling between ice volume and polar temperature over the past 150 kyr. Nature 491, 744–747.
Harding, A.E., Palutikof, J., Holt, T., 2009. The climate system. In: Woodward, J.C. (Ed.), The Physical Geography of the Mediterranean. Oxford University Press, Oxford, pp. 69–88.
Hellstrom, J., 2006. U–Th dating of speleothems with high initial ^{230}Th using stratigraphical constraint. Quaternary Geochronology 1, 289–295.
Henderson, G.M., Slowey, N.C., Fleisher, M.Q., 2001. U–Th dating of carbonate platform and slope sediments. Geochimica et Cosmochimica Acta 65, 2757–2770.
Hendy, C.H., 1971. The isotopic geochemistry of speleothems—I. The calculation of the effects of different modes of formation on the isotopic composition of speleothems and their applicability as palaeoclimatic indicators. Geochimica et Cosmochimica Acta 35, 801–824.
Hendy, C.H., Wilson, A.T., 1968. Palaeoclimatic data from speleothems. Nature 219, 48–51.
Higgins, M.D., Higgins, R.A., 1996. A Geological Companion to Greece and the Aegean. Duckworth, London (240 pp.).
Hodge, E., McDonald, J., Fischer, M., Redwood, D., Hual, Q., Levchenko, V., Drysdale, R., Waring, C., Fink, D., 2011. Using the ^{14}C bomb pulse to date young speleothems. Radiocarbon 53, 345–357.
Hodkinson, S., Hodkinson, H., 1981. Mantineia and the Mantinike: settlement and society in a Greek Polis. ABSA 76 (1981), 239–296.
Jahns, S., 1993. On the Holocene vegetation history of the Argive Plain (Peloponnese, southern Greece). Vegetation History and Archaeobotany 2, 187–203.
Jex, C.N., Baker, A., Fairchild, I.J., Eastwood, W.J., Leng, M.J., Sloane, H.J., Thomas, L., Bekaroğlu, E., 2010. Calibration of speleothem δ^{18}O with instrumental climate records from Turkey. Global and Planetary Change 71, 207–217.
Jex, C.N., Baker, A., Eden, J.M., Eastwood, W.J., Fairchild, I.J., Leng, M.J., Thomas, L., Sloane, H.J., 2011. A 500 yr speleothem-derived reconstruction of late autumn–winter precipitation, northeast Turkey. Quaternary Research 75, 399–405.
Jones, M.D., Roberts, C.N., Leng, M.J., Türkes, M., 2006. A high-resolution late Holocene lake isotope record from Turkey and links to North Atlantic and monsoon climate. Geology 34, 361–364.
Kaniewski, D., Paulissen, E., De Laet, V., Dossche, K., Waelkens, M., 2007. A high resolution Late Holocene landscape ecological history inferred from an intramontane basin in the Western Taurus Mountains, Turkey. Quaternary Science Reviews 26, 2201–2218.
Kaufman, A., Wasserburg, G.J., Porcelli, D., Bar-Matthews, M., Ayalon, A., Halicz, L., 1998. U–Th isotope systematics from the Soreq cave, Israel and climatic correlations. Earth and Planetary Science Letters 156, 141–155.
Kim, S.-T., O'Neil, J.R., 1997. Equilibrium and nonequilibrium oxygen isotope effects in synthetic carbonates. Geochimica et Cosmochimica Acta 61, 3461–3475.
Kontopoulos, N., Avramidis, P., 2003. A late Holocene record of environmental changes from the Aliki lagoon, Egion, North Peloponnesus, Greece. Quaternary International 111, 75–90.
Kouli, K., 2011. Vegetation development and human activities in Attiki (SE Greece) during the last 5,000 years. Vegetation History Archaeobotany 21, 267–278.
Kraft, J.C., Rapp Jr., G.R., Aschenbrenner, S.E., 1980. Late Holocene palaeogeomorphic reconstructions in the area of the Bay of Navarino: Sandy Pylos. Journal of Archaeological Science 7, 187–210.
Kutiel, H., Benaroch, Y., 2002. North Sea-Caspian pattern (NCP) — an upper level atmospheric teleconnection affecting the Eastern Mediterranean: identification and definition. Theoretical and Applied Climatology 71, 17–28.
Kutiel, H., Maheras, P., Türkeş, M., Paz, S., 2002. North Sea–Caspian Pattern (NCP) — an upper level atmospheric teleconnection affecting the eastern Mediterranean — implications on the regional climate. Theoretical and Applied Climatology 72, 173–192.
Lachniet, M.S., 2009. Climatic and environmental controls on speleothem oxygen-isotope values. Quaternary Science Reviews 28, 412–432.
Lambert, W.J., Aharon, P., 2011. Controls on dissolved inorganic carbon and δ^{13}C in cave waters from DeSoto Caverns: implications for speleothem δ^{13}C assessments. Geochimica et Cosmochimica Acta 75, 753–768.
Lamy, F., Arz, H.W., Bond, G.C., Bahr, A., Pätzold, J., 2006. Multicentennial-scale hydrological changes in the Black Sea and northern Red Sea during the Holocene and the Arctic/North Atlantic Oscillation. Paleoceanography 21, PA1008.
Linge, H., Baker, A., Andersson, C., Lauritzen, S.-., 2009. Variability in luminescent lamination and initial ^{230}Th/^{232}Th activity ratios in a late Holocene stalagmite from northern Norway. Quaternary Geochronology 4, 181–192.
Ludwig, K.R., Titterington, D.M., 1994. Calculation of ^{230}Th U isochrons, ages, and errors. Geochimica et Cosmochimica Acta 58, 5031–5042.
McDermott, F., 2004. Palaeo-climate reconstruction from stable isotope variations in speleothems: a review. Quaternary Science Reviews 23, 901–918.
McDermott, F., Atkinson, T.C., Fairchild, I.J., Baldini, L.M., Mattey, D.P., 2011. A first evaluation of the spatial gradients in δ^{18}O recorded by European Holocene speleothems. Global and Planetary Change 79, 275–287.
Merdenisianos, C., 2005. The cave of Kapsia at Mantinia and its anthropological findings. Hellenic Speleological Society.
Mickler, P.J., Banner, J.L., Stern, L., Asmerom, Y., Edwards, R.L., Ito, E., 2004. Stable isotope variations in modern tropical speleothems: evaluating equilibrium vs. kinetic isotope effects. Geochimica et Cosmochimica Acta 68, 4381–4393.
Mickler, P.J., Stern, L.A., Banner, J.L., 2006. Large kinetic isotope effects in modern speleothems. Bulletin of the Geological Society of America 118, 65–81.
Orland, I.J., Bar-Matthews, M., Kita, N.T., Ayalon, A., Matthews, A., Valley, J.W., 2009. Climate deterioration in the Eastern Mediterranean as revealed by ion microprobe analysis of a speleothem that grew from 2.2 to 0.9 ka in Soreq Cave, Israel. Quaternary Research 71, 27–35.
Parker, C., 2006. Arkadian landscapes. Rosetta 1, 10–21.
Pitsios, T., 1984. Η ανθρωπολογική μελέτη των σκελετικών ευρημάτων αρχαιολογικών ανασκαφών. Ανθρωπολογικά 6, 41–51.
Pitsios, T., Ioannou, I., Merdenisianos, K., 1995. 5th International Congress on Cave Development, Evolution and Environment. Deltion ESE, vol. XXI, p. 201 (Athens).
Psathi, E., 2004. Σπήλαιο Κάψια. Archaeologicon Deltion 56–59 (2001–2004), 522.
Richards, D.A., Dorale, J.A., 2003. Uranium-series chronology and environmental applications of speleothems. Reviews in Mineralogy and Geochemistry 52, 407–460.
Roberts, N., Reed, J.M., Leng, M.J., Kuzucuoglu, C., Fontugne, M., Bertaux, J., Woldring, H., Bottema, S., Black, S., Hunt, E., Karabiyikoglu, M., 2001. The tempo of Holocene climatic change in the eastern Mediterranean region: new high-resolution crater-lake sediment data from central Turkey. The Holocene 11, 721–736.
Roberts, N., Jones, M.D., Benkaddour, A., Eastwood, W.J., Filippi, M.L., Frogley, M.R., Lamb, H.F., Leng, M.J., Reed, J.M., Stein, M., Stevens, L., Valero-Garcés, B., Zanchetta, G., 2008. Stable isotope records of Late Quaternary climate and hydrology from Mediterranean lakes: the ISOMED synthesis. Quaternary Science Reviews 27, 2426–2441.
Roberts, N., Eastwood, W.J., Kuzucuoğlu, C., Fiorentino, G., Caracuta, V., 2011. Climatic, vegetation and cultural change in the eastern Mediterranean during the mid-Holocene environmental transition. The Holocene 21, 147–162.
Schilman, B., Almogi-Labin, A., Bar-Matthews, M., Labeyrie, L., Paterne, M., Luz, B., 2001. Long- and short-term carbon fluctuations in the Eastern Mediterranean during the late Holocene. Geology 29, 1099–1102.
Schilman, B., Almogi-Labin, A., Bar-Matthews, M., Luz, B., 2003. Late Holocene productivity and hydrographic variability in the eastern Mediterranean inferred from benthic foraminiferal stable isotopes. Paleoceanography 18.
Thiébault, F., Fleury, J.J., Clément, B., Dégardin, J.M., 1994. Paleogeographic and paleotectonic implications of clay mineral distribution in late Jurassic–early Cretaceous sediments of the Pindos–Olonos and Beotian Basins, Greece. Palaeogeography, Palaeoclimatology, Palaeoecology 108, 23–40.
Thornthwaite, C.W., 1954. The measurement of potential evapotranspiration. Mather, Seabrook, NJ (225 pp.).
Torrence, C., Compo, G.P., 1998. A practical guide to wavelet analysis. Bulletin of the American Meteorological Society 79, 61–78.
Tremaine, D.M., Froelich, P.N., Wang, Y., 2011. Speleothem calcite farmed in situ: modern calibration of δ^{18}O and δ^{13}C paleoclimate proxies in a continuously-monitored natural cave system. Geochimica et Cosmochimica Acta 75, 4929–4950.

https://doi.org/10.1016/j.yqres.2013.12.009 Published online by Cambridge University Press

Triantaphyllou, M.V., Kouli, K., Tsourou, T., Koukousioura, O., Pavlopoulos, K., Dermitzakis, M.D., 2010. Paleoenvironmental changes since 3000 BC in the coastal marsh of Vravron (Attica, SE Greece). Quaternary International 216, 14–22.
Türkeş, M., Erlat, E., 2003. Precipitation changes and variability in Turkey linked to the North Atlantic oscillation during the period 1930–2000. International Journal of Climatology 23, 1771–1796.
Unkel, I., Schimmelmann, A., Shriner, C., Forsén, J., Heymann, C., Brückner, H., 2013. The environmental history of the last 6500 years in the Asea Valley (Peloponnese, Greece) and its linkage to the local archaeological record. Zeitschrift für Geomorphologie (in press).
Urban, B., Fuchs, M., 2005. Late Pleistocene vegetation of the basin of Phlious, NE-Peloponnese, Greece. Review of Palaeobotany and Palynology 137, 15–29.
Verheyden, S., Nader, F.H., Cheng, H.J., Edwards, L.R., Swennen, R., 2008. Paleoclimate reconstruction in the Levant region from the geochemistry of a Holocene stalagmite from the Jeita Cave, Lebanon. Quaternary Research 70, 368–381.
Wick, L., Lemcke, G., Sturm, M., 2003. Evidence of Lateglacial and Holocene climatic change and human impact in eastern Anatolia: high-resolution pollen, charcoal, isotopic and geochemical records from the laminated sediments of Lake Van, Turkey. The Holocene 13, 665–675.
Zanchetta, G., Drysdale, R.N., Hellstrom, J.C., Fallick, A.E., Isola, I., Gagan, M.K., Pareschi, M.T., 2007. Enhanced rainfall in the Western Mediterranean during deposition of sapropel S1: stalagmite evidence from Corchia cave (Central Italy). Quaternary Science Reviews 26, 279–286.
Zangger, E., Timpson, M.E., Yazvenko, S.B., Kuhnke, F., Knauss, J., 1997. The Pylos regional archaeological project: part II: landscape evolution and site preservation. Hesperia 66, 549–641.

Further reading

Bar-Matthews, M., Ayalon, A., Matthews, A., Sass, E., Halicz, L., 1996. Carbon and oxygen isotope study of the active water-carbonate system in a karstic Mediterranean cave: implications for paleoclimate research in semiarid regions. Geochimica et Cosmochimica Acta 60, 337–347.
Caseldine, C.J., Turney, C., 2010. The bigger picture: towards integrating palaeoclimate and environmental data with a history of societal change. Journal of Quaternary Science 25, 88–93.
Fleitmann, D., Burns, S.J., Neff, U., Mudelsee, M., Mangini, A., Matter, A., 2004. Palaeoclimatic interpretation of high-resolution oxygen isotope profiles derived from annually laminated speleothems from Southern Oman. Quaternary Science Reviews 23, 935–945.
Kaniewski, D., Paulissen, E., Van Campo, E., Al-Maqdissi, M., Bretschneider, J., Van Lerberghe, K., 2008. Middle East coastal ecosystem response to middle-to-late Holocene abrupt climate changes. Proceedings of the National Academy of Sciences of the United States of America 105, 13941–13946.

https://doi.org/10.1016/j.yqres.2013.12.009 Published online by Cambridge University Press